Experimental and theoretical investigation of the influence of heat transfer rate on the thermal performance of a multi-channel flat heat pipe

Valentin Guichet [a], Bertrand Delpech [a], Navid Khordehgah [a], Hussam Jouhara [a, b, *]

[a] *Heat Pipe and Thermal Management Research Group, College of Engineering, Design and Physical Sciences, Brunel University London, UB8 3PH, UK*
[b] *Vytautas Magnus University, Studentu, Kaunas, Lithuania*

ARTICLE INFO

ABSTRACT

Recently, flat heat pipes have been proposed for surface cooling applications to passively extract and recover thermal energy from hot surfaces. For instance, flat heat pipes have recently been proposed as thermal absorber for photovoltaic/thermal (PV/T) applications or for the thermal management of batteries. Following promising surface cooling results, increasing the fundamental knowledge of the two-phase heat transfer taking place inside such multi-channel flat heat pipes can participate to its widespread and lead to further improvement of the technology. Indeed, until now, the investigations have focused on the application only and not on the performance of the flat heat pipe itself. In this regard, this manuscript experimentally and theoretically investigates the thermal performance of a multi-channel flat heat pipe used for surface cooling applications. Heat transfer rates in the range 0–1500 W are studied and their impact on the boiling, condensation, and total thermal resistance of the multi-channel flat heat pipe is measured. In order to predict the thermal performance of the multi-channel flat heat pipe at all heat transfer rates, a theoretical model is proposed, which considers the impact of the multi-channel geometry. This model uses a multi-channel thermal resistance network. Furthermore, an important number of two-phase correlations for pool boiling and condensation are compared with experimental data and the optimum equations are integrated into the multi-channel model. As a result, over the whole range of heat transfer rates investigated, the proposed multi-channel flat heat pipe model was able to predict the boiling, condensation, and total thermal resistances of the heat pipe with an average error of 17.2%, 14.4% and 13.1%, respectively. Finally, the impact of the tilt angle is also studied, and infrared imaging of the flat heat pipe surface is presented.

1. Research background

Thermal absorbers have been used to extract and recover the excess heat from flat surfaces with the objective of maintaining an optimum temperature of photovoltaic cells and batteries. Due to their high thermal conductivity and uniform temperature distribution characteristics, heat pipes have been proposed as a technical solution for surface cooling purposes [1]. However, to assure the two-phase cycle of the working fluid, heat pipes are commonly manufactured with cylindrical shapes which is not suitable for surface cooling applications. In this regard, flat heat pipes have recently appeared that use an internal multi-channel geometry in which the working fluid transfers the thermal energy. Such flat heat pipes have appeared in two surface cooling applications: photovoltaic/thermal (PV/T) panels, and battery thermal management [2–5].

One of the first uses of a flat heat pipe for the cooling of photovoltaic (PV) cells was reported by *Deng* et al. [6] who presented a flat micro heat pipe array made in aluminium. The internal geometry of the flat heat pipe consisted of eight independent parallel channels with micro fins. However, due to the limited width of the flat heat pipe used (about 50 mm), several independent heat pipes were placed in parallel for the cooling of the PV panel. In this case, a uniform temperature distribution of the apparatus was only partially achieved. A water tube combined with

* Corresponding author. Heat Pipe and Thermal Management Research Group, College of Engineering, Design and Physical Sciences, Brunel University London, UB8 3PH, UK.

E-mail address: hussam.jouhara@brunel.ac.uk (H. Jouhara).

Nomenclature

A	Surface area m^2
C	Constant Dimensionless
c_p	Specific heat $J.kg^{-1}.K^{-1}$
C_{sf}	Constant in Rohsenow correlation depending on the surface-fluid combination Dimensionless
D	Diameter m
D_d	Bubble departure diameter m
g	Gravitational acceleration $m.s^{-2}$
h	Heat transfer coefficient $W.m^{-2}.K^{-1}$
i_{lv}	Latent heat of vaporization $J.kg^{-1}$
Ja	Jakob number, $(Ja = \Delta T c_{p,l} \rho_l / \rho_v i_{lv})$ dimensionless
k	Thermal conductivity $W.m^{-1}.K^{-1}$
L	Length m
L_b	Bubble length scale, $(L_b = [\sigma/g(\rho_l - \rho_v)]^{1/2})$ m
$\dot{m}$	Mass flow rate $kg.s^{-1}$
M_{mol}	Molecular weight $kg.kmol^{-1}$
N_a	Number of active nucleation sites per unit surface area m^{-2}
N_{mol}	Avogadro number, $(N_{mol} = 6.022 \times 10^{20})$ $kmol^{-1}$
P	Pressure Pa
P^*	Dimensionless reduced pressure, $(P^* = P/P_{crit})$ $N.m^{-2}$
Pr	Prandtl number, $(Pr = c_p \mu / k)$ Dimensionless
$\dot{Q}$	Heat transfer rate W
$q^{''}$	Heat flux per surface unit area $W.m^{-2}$
R	Thermal resistance $K.W^{-1}$
R_a	Arithmetic mean deviation of the profile (Mittenräuwert), ISO4287-1 : 1984/DIN4762 m
$R_{a,p}$	Average roughness parameter μm
Re_f	Falling film Reynolds number, $(Re_f = 4\Gamma/\mu_l)$ Dimensionless
R_{mol}	Molar specific gas constant, $(R_{mol} = 8314.4598)$ $J.K^{-1}.kmol^{-1}$
S_x	Uncertainty related to the variable x Unit of x
T	Temperature K
w	Pitch m
z	Thickness m

Greek Symbols

α	Thermal diffusivity, $(\alpha = k/\rho c_p)$ $m^2.s^{-1}$
δ	Film thickness m
Δ	Difference Dimensionless
Γ	Mass rate of liquid flow per unit periphery $kg.m^{-1}.s^{-1}$
ρ	Density $kg.m^{-3}$
σ	Surface tension $N.m^{-1}$
μ	Dynamic viscosity Pa.s

Subscripts

$Alum$	Aluminium
$boiling$	Boiling
c	Condenser/Condensation
$condensation$	Condensation
e	Evaporator
ffb	Falling film boiling
in	Inlet
$manifold$	Cooling manifold
pb	Pool boiling
out	Outlet
s	Surface
sat	Saturation
v	Vapour
w	Wall
$water$	Water

Superscripts

$''$	Per surface area m^{-2}
$\cdot$	Per unit of time s^{-1}
$*$	Dimensionless variable, dimensionless

Acronyms

FR	Filling ratio
HP	Heat pipe
PV/T	Photovoltaic/thermal

a flat heat exchanger was used as a heat sink. After a year of investigation, the maximum combined photovoltaic-thermal efficiency was recorded at 45.5%, with 31.6% thermal efficiency and 13.4% electrical efficiency. Another study made by the same group of researchers was published by *Hou* et al. [7] and revealed that the thermal efficiency of their apparatus was greatly influenced by the cooling water temperature inside the tank. Thus, between summer and winter, the thermal efficiency of the heat pipe based photovoltaic/thermal (PV/T) system decreased from 40% to 20%. A similar micro-heat pipe array was used by *Modjinou* et al. [8] who used six parallel flat heat pipes charged with acetone for the cooling of their PV cells. The daily electrical and thermal efficiencies measured were 7.6% and 50.7%. Yet, in the previous investigations where several micro-heat pipe arrays were used for cooling photovoltaic cells, the independent operation of each flat heat pipe means that they can present different working temperatures. Thus, the cooling of the photovoltaic cells is not uniform. In particular, with the warmup of the cooling water inside the heat sink, it is very likely that significant temperature differences occurred between the flat heat pipes placed near the water inlet and those near the water outlet. In a different PV/T application, *Shittu* et al. [9] used a flat plate micro-channel heat pipe at the back of their photovoltaic cells. In this apparatus, the authors chose to combine the flat heat pipe with a thermoelectric generator which converted the thermal energy extracted to electricity. In this study, low interest was given to thermal energy and the aim was the maximising of the electrical output. Nevertheless, the thermal efficiency of the system was measured, and the maximum efficiency reached 69.5%. Unfortunately, in this work, very little information on the flat plate micro-channel heat pipe was provided. *Yu* et al. [10] investigated the thermal performance of a multi-channel flat heat pipe made of twenty micro-channel heat pipes linked at the top and bottom by headers for cooling photovoltaic cells. Several limits can be identified in the proposed system. For instance, empty spaces were found between each parallel micro-channel heat pipe, which shows that the whole absorber surface was not passively active. Further, an aluminium plate was used between the multi-channel heat pipes and the PV cells, which has the advantage of improving the cooling uniformity but increases the thermal resistance of the absorber. The thermal efficiency of the multi-channel flat heat pipe-based absorber was found to be in the range 25.2%–62.2%. To tackle the non-uniform temperature distribution of heat pipes

using independent channels, *Jouhara* et al. [4,11] designed and patented a multi-channel flat heat pipe called "Heat Mat" which uses parallel channels connected by collectors and allows the circulation of the working fluid in all the channels. In addition, the heat mat uses a unique channel shape to enhance the heat transfer from a flat heat source to the working fluid. By using the heat mat as a built-in integrated material, the temperature of the photovoltaic cells was decreased from a range of 40−58 °C to 28−33 °C, which led to an increase of the electrical output of 15%. As a result, the multi-channel flat heat pipe-based PV/T system reached electrical and thermal efficiencies of 6.1% and 64%, respectively. Yet, to date the performance of the heat mat has only been investigated experimentally.

The thermal management of batteries is another area in which multi-channel flat heat pipes have recently been introduced as a technical solution. If the temperature of the battery is not controlled, a loss of efficiency in terms of functionality and capacity is observed [12]. In addition, failing to balance the change of battery temperature generated by the internal chemical reactions decreases the life cycle and safety of the batteries [2]. In this regard, *Jouhara* et al. [3] used a multi-channel flat heat pipe (heat mat) for the temperature control of batteries. Due to the internal geometry of the parallel channels linked at the top and bottom by collectors, the battery temperature was uniformly maintained within ±1 °C. It was demonstrated that the heat mat was able to remove about 60% of the heat generated by the battery and that the maximum battery temperature reached only 28 °C. *Diao* et al. [13] presented a new type of latent heat thermal energy storage in which the phase change material was in contact with six flat micro-heat pipe arrays. The flat heat pipe array comprised parallel channels inside which the heat transfer area between the wall and the working fluid was increased by using fins. Unfortunately, the thermal performance of the flat micro-heat pipe arrays was not evaluated. *Zhao* et al. [14] studied the temperature management of lithium-ion batteries using flat heat pipes. Even if the internal geometry of the flat heat pipes used was not described, the parallel micro-channels are likely to be connected. The flat heat pipes were 2 mm thick, made from aluminium extrusions, and they used acetone as the working fluid. Different types of heat sinks for the heat pipes were compared and it was found that the horizontal heat pipes with wet cooling was the system which managed to keep the lowest battery temperature. Indeed, the temperature of the packs was maintained below 30 °C with a maximum temperature difference of 1.5 °C within the battery pack.

Despite the recent introduction and promising results of multi-channel flat heat pipes with surface cooling applications, to date most of the published work focuses on the application and not on the thermal performance of the multi-channel flat heat pipe itself. In particular, the number of theoretical models of multi-channel flat heat pipes in the literature is limited. *Almahmoud and Jouhara* [15,16] and *Delpech* et al. [17] are the only authors who proposed theoretical models of multi-channel heat pipes. In both cases, the multi-channel heat pipes modelled consisted of cylindrical stainless-steel tubes linked at the top and bottom by collectors. In their theoretical models, the authors considered an equivalent heat transfer area of boiling and condensation and thus assumed a constant temperature between each leg and the collectors. Recently, *Guichet* et al. [18] investigated the thermal performance of a multi-channel flat heat pipe and proposed a theoretical model which considers the multi-channel geometry. At a heat transfer rate of 500 W, the temperature of the heat pipe was predicted within a 1.4 °C error and the multi-channel flat heat pipe thermal resistance within a 30% error. Yet, so far, only one heat transfer rate was investigated, and the multi-channel flat heat pipe model proposed remains to be further validated at different heat transfer rates.

Following a previous publication by *Guichet* et al. [18], the multi-channel flat heat pipe theoretical model proposed must be further validated by investigating different heat transfer rates. Hence, in this paper, the thermal performance of a multi-channel flat heat pipe is investigated at various heat transfer rates in a range 0−1500 W. The proposed theoretical model is also optimized by comparing the various pool boiling and condensation correlations to be introduced in the multi-channel thermal resistance model. The capacity of the model to predict the thermal performances of the multi-channel flat heat pipe is investigated. Finally, to increase the knowledge on two-phase heat transfer in multi-channel flat heat pipes, the impact of the tilt angle on the thermal performance is also studied, and infrared red imaging of the flat heat pipe is presented.

2. Experimental apparatus

The multi-channel flat heat pipe (heat mat) investigated presents a rectangular flat surface of 680 × 497mm, a thickness of 12 mm, and comprises 43 vertical parallel channels obtained by aluminium extrusion. The parallel channels are linked at the top and bottom by horizontal collectors, which allow the circulation of the working fluid in all the channels. The channels' cross section fits in a circle of diameter 6 mm. For more details on the internal structure of the multi-channel flat heat pipe, insights are provided in the International Patent n° WO2015193683 [19]. In this study, R134a was used as a working fluid. Based on the size of the evaporator, in this experiment, the filling ratio FR was 100% which means that the complete evaporator was filled by the liquid pool. Flat silicon heaters were placed as a heat source at the bottom of the multi-channel flat heat pipe surface. At the top of the heat mat, a cooling manifold inside which water circulates recovered the thermal energy distributed by the heat pipe. High conductivity thermal paste was used to decrease the contact resistance between the heat pipe and the flat elements. The multi-channel flat heat pipe assembly and heat transfer principles of the device investigated are presented in Fig. 1.

To measure the performance of the heat pipe, thermocouples were placed on the heat pipe at 16 different locations and all the system was covered with insulation to prevent thermal losses. The thermocouple locations are presented in Fig. 2. Due to the presence of the heaters and cooling manifold on the front surface, the temperature measurements for evaporator and condenser sections had to be made from the back surface of the flat heat pipe.

With the objective of investigating the impact of the heat transfer rate on the performance of the multi-channel flat heat pipe, the power was adjusted via a control box and measured with a power logger PEL105. The heat transfer rate range investigated was selected to be 0−1500 W and an incremental step of 100 W was
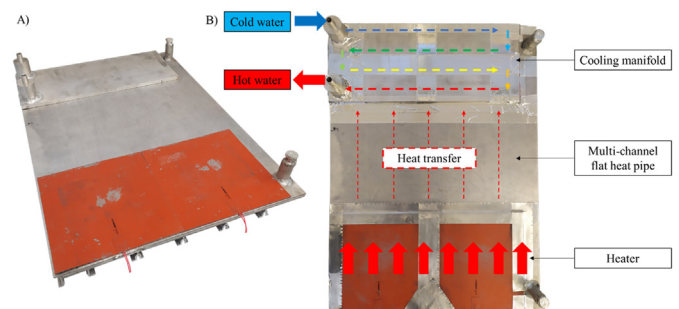

Fig. 1. A) Multi-channel flat heat pipe assembly and B) heat transfer principles of the investigated multi-channel flat heat pipe test rig.
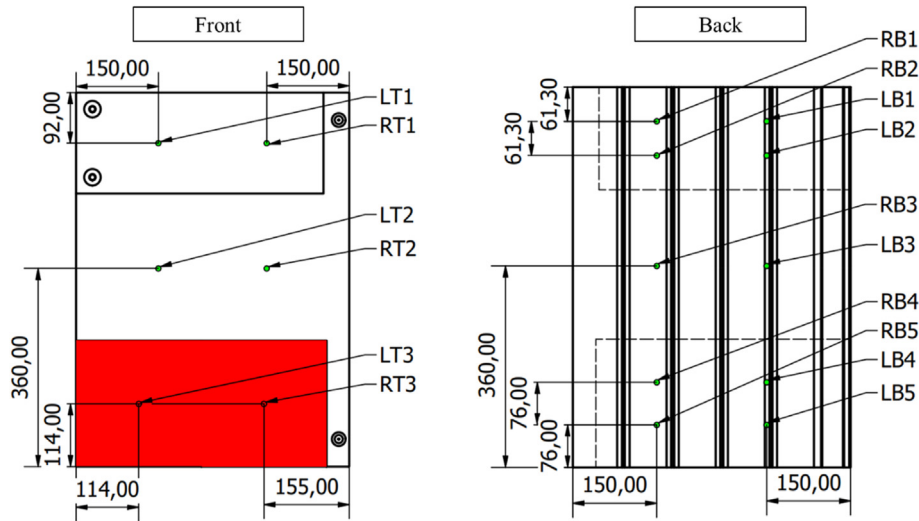
Fig. 2. Thermocouple locations.

used. Four thermocouples were placed on the cooling water inlet and outlet to measure the heat transfer rate experimentally. The test apparatus also allowed the control of the cooling water flow rate using a valve. The flow rate was measured manually by multiple (6 or 7) cooling water volume samples. The heat pipe was placed on a rotating axis so that the tilt angle of the apparatus could be changed. Finally, temperature measurements from the thermocouples were recorded using two NI-9213 thermocouple modules and a national instrument datalogger. The experimental test rig used is presented in Fig. 3.

3. Data reduction

In the objective of describing the thermal performance of the multi-channel flat heat pipe, the raw data from the thermocouples and cooling water flow rate measurements are reduced to other quantifiable parameters. The experimental heat transfer rate passing through the system can be obtained using the cooling water mass flow rate and temperature measurements for water inlet and outlet:

Fig. 3. Experimental test rig.

$$\dot{Q} = \dot{m}_{water} c_{p,water} \left(T_{water,\, out} - T_{water,\, in} \right) \tag{1}$$

where $\dot{Q}$ is the heat transfer rate through the system (W), $\dot{m}_{water}$ is the water flow rate in the cooling manifold (kg/s), $c_{p,water}$ is the specific heat of water (J/kg.K), and $T_{water,\, out}$ and $T_{water,\, in}$ are the water temperatures at the outlet and inlet (K), respectively. To avoid potential errors in the modelling of the multi-channel flat heat pipe, in this study the thermal resistance of the cooling manifold was determined experimentally from:

$$R_{cooling\ manifold} = \frac{1}{\dot{Q}} \times \frac{T_{water,in} - T_{water,out}}{ln\left((T_s - T_{water,out}) / (T_s - T_{water,in}) \right)} \tag{2}$$

where $R_{coolingmanifold}$ is the cooling manifold thermal resistance (K/W), $\dot{Q}$ is the total heat transfer rate through the system (W), $T_{water,in}$ and $T_{water,out}$ are the water inlet and outlet temperatures (K), and T_s is the surface temperature of cooling manifold in contact with the heat pipe (K). Averages of the thermocouples in the relevant zone were calculated to determine the temperature of the evaporator, adiabatic, and condenser sections of the flat heat pipe. Then, the boiling, condensation, and total thermal resistances of the multi-channel flat heat pipe were obtained from:

$$R_{boiling} = \frac{(T_{evaporator} - T_{adiabatic})}{\dot{Q}} \tag{3}$$

$$R_{condensation} = \frac{(T_{adiabatic} - T_{condenser})}{\dot{Q}} \tag{4}$$

$$R_{HP} = \frac{(T_{evaporator} - T_{condenser})}{\dot{Q}} \tag{5}$$

where $R_{boiling}$, $R_{condensation}$, and R_{HP} are the boiling, condensation, and total heat pipe thermal resistances (K/W), $T_{evaporator}$, $T_{adiabatic}$, and $T_{condenser}$ the evaporator, adiabatic, and condenser temperatures (K), and $\dot{Q}$ the heat transfer rate (W). Experimentally, the boiling and condensation heat transfer coefficients can be derived from the respective thermal resistances with:
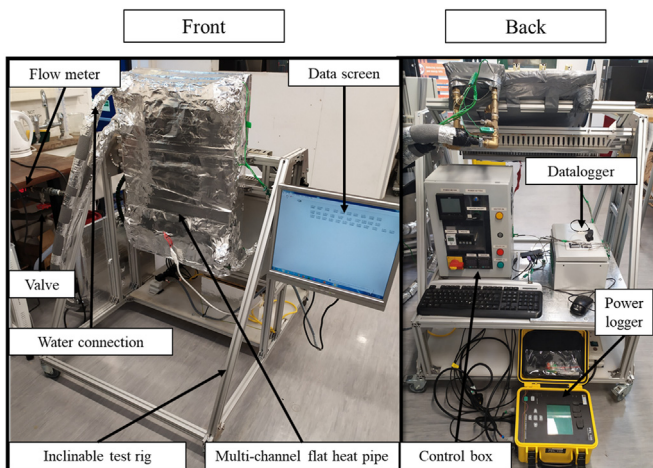
$$h = \frac{1}{AR} \tag{6}$$

with h the heat transfer coefficient (W/m^{2}K), A the heat transfer area (m^2), and R the thermal resistance (K/W).

4. Error propagation and standard deviation

The accuracy of the experimental results was estimated from the propagation of measurement errors in the experimental data from the sensors. To estimate the error from the experiments, two strategies are possible and they are compared. On the one hand, the error can be estimated theoretically by considering the uncertainty from the sensors and studying the propagation of the errors in the data reduction equation. On the other hand, the experimental error can be assessed by studying the standard deviation between multiple experiments. This approach mainly estimates the scatter of the data but does not detect systematic errors. Starting with the measurement uncertainty, the temperature measurement error from the thermocouples was estimated by operating a series of 10 measurements on 5 different K-type thermocouples inside cold and boiling water. The uncertainty from the cooling water flow rate measurement was estimated by repeating the measurement of the same water flow rate 10 times. The estimated measurement uncertainties are reported in Table 1 below.

From the estimated uncertainties of the temperature and flow rate measurements, the possible error in estimating the heat transfer rate $S_{\dot{Q}}$ can be calculated from:

$$S_{\dot{Q}} = \dot{Q} \sqrt{\left(\frac{S_{\dot{m}_{water}}}{\dot{m}_{water}}\right)^2 + \left(\frac{S_{\Delta T_{water}}}{\Delta T_{water}}\right)^2} \tag{7}$$

$$S_{\Delta T_{water}} = \sqrt{S_{T_{water,\,out}}{}^2 + S_{T_{water,\,in}}{}^2} = S_T \tag{8}$$

with $\dot{Q}$ the heat transfer rate (W), $S_{\dot{m}_{water}}$ the uncertainty related to the water mass flow rate $\dot{m}_{water}$ (kg/s), $S_{\Delta T_{water}}$ the uncertainty related to the difference of cooling water temperature (K), and $S_{T_{water,\,out}}$ and $S_{T_{water,\,in}}$ the error uncertainties related to the water outlet and water inlet temperature measurements (K). The error related to the cooling manifold thermal resistance $S_{R_{cooling\ manifold}}$ is given by:

$S_{\dot{Q}}$ the uncertainty related to the heat transfer rate $\dot{Q}$ (W), $S_{\Delta T_{water}}$ the uncertainty related to the cooling water difference of temperature ΔT_{water} (K), S_T the thermocouple uncertainty (K), T_s the cooling manifold surface temperature in contact with the heat pipe (K), and $T_{water,in}$ and $T_{water,out}$ are the water inlet and outlet temperatures (K). To estimate the uncertainty on the boiling, condensation, and total heat pipe thermal resistances, the following equations are used:

$$S_{R_{boiling}} = R_{boiling} \sqrt{\frac{S_{T_{evaporator}}{}^2 + S_{T_{adiabatic}}{}^2}{\left(T_{evaporator} - T_{adiabatic}\right)^2} + \left(\frac{S_{\dot{Q}}}{\dot{Q}}\right)^2} \tag{10}$$

$$S_{R_{condensation}} = R_{condensation} \sqrt{\frac{S_{T_{adiabatic}}{}^2 + S_{T_{condenser}}{}^2}{\left(T_{adiabatic} - T_{condenser}\right)^2} + \left(\frac{S_{\dot{Q}}}{\dot{Q}}\right)^2} \tag{11}$$

$$S_{R_{HP}} = R_{HP} \sqrt{\frac{S_{T_{evaporator,pb}}{}^2 + S_{T_{condenser}}{}^2}{\left(T_{evaporator,pb} - T_{condenser}\right)^2} + \left(\frac{S_{\dot{Q}}}{\dot{Q}}\right)^2} \tag{12}$$

In the above equations, $R_{boiling}$, $R_{condensation}$, and R_{HP} are the boiling, condensation, and total heat pipe thermal resistances (K/W), $T_{evaporator}$, $T_{adiabatic}$, and $T_{condenser}$ the evaporator, adiabatic, and condenser temperatures (K), and $\dot{Q}$ the heat transfer rate (W) and S_x the corresponding uncertainty of the variable x.

Based on the data reduction equation, the data error was estimated theoretically. This estimated error on the data was compared with the experimental error which was obtained by doing the standard deviation between four similar experiments. In Fig. 4 are presented the theoretical and experimental errors made in the estimation of the heat transfer rate and of the cooling manifold at heat transfer rates in the range 0−1500 W.

Based on the error propagation equation, the maximum relative error made on the estimation of the heat transfer rate is about 25% and it is obtained at a minimum heat transfer rate of 100 W. Experimentally, the standard deviation between the four experiments that were conducted at a heat transfer rate of 100 W was 10%. Hence, the experimental error observed seems to be lower than the expected theoretical error, which means that the experimental data can be repeated with similar results and confirms the

$$S_{R_{cooling\ manifold}} = R_{cooling\ manifold} \times \sqrt{\left(\frac{S_{\dot{Q}}}{\dot{Q}}\right)^2 + \left(\frac{S_{\Delta T_{water}}}{\Delta T_{water}}\right)^2 + \left(\frac{\sqrt{\frac{\sfrac{3}{4}S_T{}^2}{(T_s - T_{water,out})^2} + \frac{\sfrac{3}{4}S_T{}^2}{(T_s - T_{water,in})^2}}}{ln\left((T_s - T_{water,out})/(T_s - T_{water,in})\right)}\right)^2} \tag{9}$$

with $R_{cooling\ manifold}$ the cooling manifold thermal resistance (K/W),

accuracy of the results. Similar observations were made while determining the cooling manifold thermal resistance during which the theoretical error was expected to be as high as 50% whereas, experimentally, the cooling manifold thermal resistance calculated was not varying by more than 10% between four similar experiments. More importantly for the current study, the experimental error on the data was relatively low for the heat pipe thermal

Table 1
Estimated measurement uncertainties.

Flow rate manual measurement	$S_{V_{waterin10s,manual}}$	2.5 ml
Thermocouple	S_T	0.2 K

Theoretical and experimental errors - Heat transfer rate

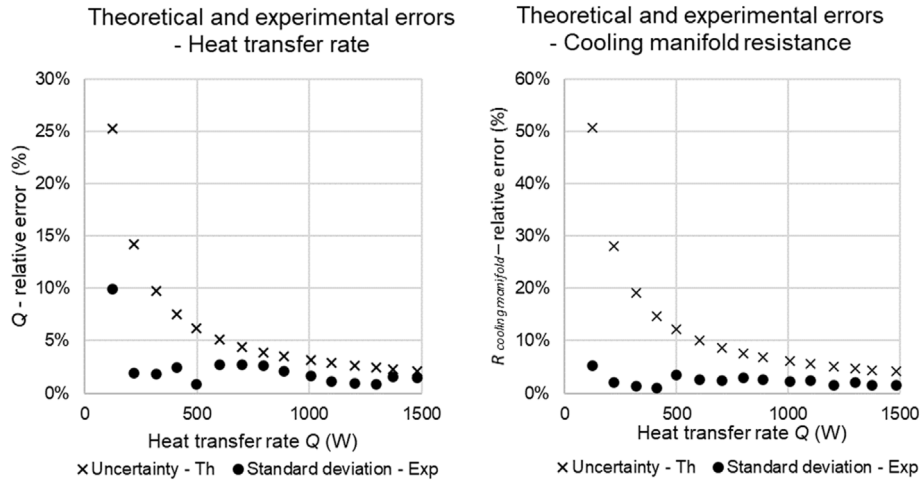Theoretical and experimental errors - Cooling manifold resistance

Fig. 4. Theoretical and experimental errors of the heat transfer rate and cooling manifold resistance during the multi-channel flat heat pipe experiments.
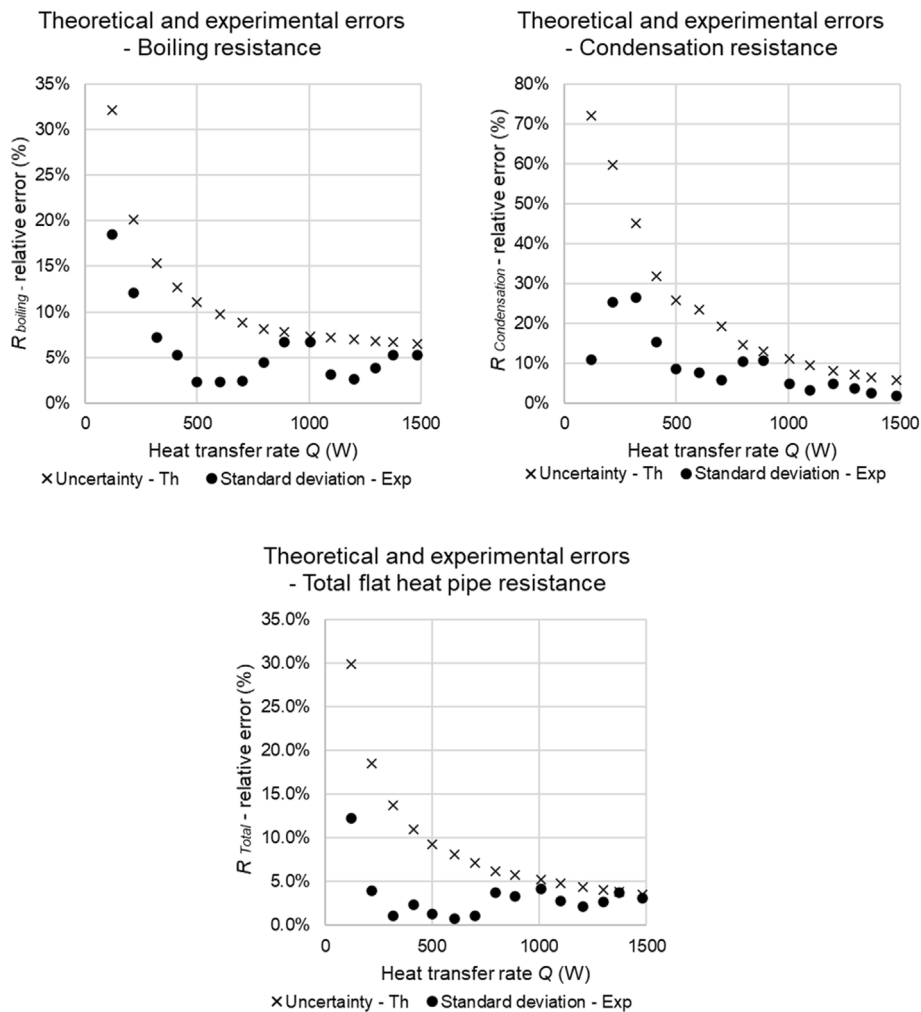
Theoretical and experimental errors - Boiling resistance

Theoretical and experimental errors - Condensation resistance

Theoretical and experimental errors - Total flat heat pipe resistance

Fig. 5. Theoretical and experimental errors of the boiling, condensation, and total flat heat pipe thermal resistance during the multi-channel flat heat pipe experiments.

resistances too, as witnessed by Fig. 5.

Overall, it is observed that the experimental error decreases with an increase of the heat transfer rate. This is explained as an increase of the heat transfer rate generates higher differences of temperature inside the system which reduces the relative error of the temperature measurements from the thermocouples. Theoretically, the condensation thermal resistance error was estimated to be relatively high due to very low differences of temperatures

between the adiabatic and condenser sections. In comparison, for the boiling thermal resistance, the difference of temperature between the evaporator and adiabatic section is high and thus, the expected and measured errors are lower. Even if, based on the estimated inaccuracy of the measurements and of the data reduction equation, the error made on the boiling and condensation thermal resistances is expected to be up to 33% and 72%, experimentally, the standard deviation between the experiments shows a standard deviation lower than 20% for the boiling thermal resistance and lower than 30% for the condensation thermal resistance. A maximum standard deviation of 13% was observed while determining the total heat pipe thermal resistance. Hence, the analysis of the experimental error shows that the estimated experimental error is higher than the measured experimental error of the data. The low standard deviation observed in the experimental results shows a satisfying repetition of the experiments and brings confidence in the accuracy of the results obtained.

5. Theoretical model

Theoretical models are available in the case of single cylindrical thermosyphons (wickless heat pipes). Despite the complex two-phase mechanisms involved in the evaporation and condensation of the working fluid inside the heat pipe, several correlations have been identified as reliable in predicting the performance of heat pipes [20,21]. To estimate the pool boiling heat transfer coefficient, the correlation by *Rohsenow* [22] is usually used whereas the *Nusselt* [23] correlation is employed to describe the film condensation heat transfer. By using a thermal resistance analysis, these correlations allow a determination of the temperature inside the heat pipe. In the case of a multi-channel heat pipe, which comprises parallel legs linked by top and bottom collectors, a thermal resistance network must be adapted. Hence, in this manuscript, a new thermal resistance network is proposed which includes the parallel legs and the two collectors. The equivalent thermal resistance model proposed for the multi-channel flat heat pipe is presented in Fig. 6.

In the above thermal resistance model, R_{ext} is the external thermal resistance, $R_{wall,e\ channel}$ is the conduction thermal resistance at the evaporator to a single channel, $R_{wall,e\ bottom\ collector}$ is the conduction thermal resistance at the evaporator to the bottom collector. Similar thermal resistances are included at the condenser

section. Those resistances are calculated using well known conduction equations. For each channel, the conduction thermal resistance is given by Ref. [24]:

$$R_{conduction-1\ channel} = \frac{\ln\left(\frac{2w}{\pi D} \sinh \frac{2\pi z}{w}\right)}{k_{alum} 2\pi L} \ (for\ each\ channel) \qquad (13)$$

with w the distance between each channel (m), D the channel diameter (m), z the distance between the heat pipe surface and the channel axis (m), k_{alum} the thermal conductivity of aluminium (W/m.K), and L the length of a channel (m). The two-phase thermal resistances comprise the falling film boiling thermal resistance R_{ffb}, the pool boiling thermal resistance R_{pb}, and the condensation thermal resistance R_c. To estimate those two-phase thermal resistances, the corresponding heat transfer coefficient must be predicted as the two-phase thermal resistance R is related to the heat transfer coefficient by:

$$R = \frac{1}{Ah} \qquad (14)$$

with A the heat transfer area (m²), and h the two-phase heat transfer coefficient (W/m²K). Many correlations have been proposed in the literature for calculating boiling and condensation heat transfer coefficients [20,21]. Each correlation has been developed under different conditions, with various working fluids and metal surfaces. As a result, the accuracy of the two-phase correlations varies a lot, and it is common practice for researchers to compare the different two-phase correlations with their experimental data. In the case of the multi-channel flat heat pipe studied, falling film boiling was not present due to the height of the heat source. Hence, only pool boiling and condensation correlations were compared. The pool boiling correlations compared are listed in Table 2.

Regarding the filmwise condensation correlation, the heat transfer coefficient is highly related to the thickness of the film and of the turbulence within the falling film. Indeed, a thin and turbulent film will present much higher heat transfer potential than a thick and non-turbulent film. Hence, to characterize the turbulence of the falling film, as with convective heat transfer, the falling film is characterized by a film Reynolds number Re_{f,L_c}:

$$Re_{f,L_c} = \frac{4\Gamma_{L_c}}{\mu_l} = \frac{4}{\mu_l} \frac{k_l(T_{sat}-T_w)}{i_{lv}\delta} L_c = h_{Nusselt} \frac{4(T_{sat}-T_w)L_c}{\mu_l i_{lv}} \qquad (15)$$

In the above equation, Γ_{L_c} is the mass rate of liquid flow per unit periphery over the condenser length (kg/m.s), μ_l is the liquid dynamic viscosity (Pa.s), k_l the liquid thermal conductivity (W/m.K), T_{sat} the saturation temperature (K), T_w the wall temperature (W), i_{lv} the latent heat of vaporization (J/kg), δ the film thickness (m), L_c the condenser length (m), and $h_{Nusselt}$ the *Nusselt* [23] heat transfer coefficient (W/m².K). In his work, *Nusselt* [23] presented a theory relating the heat transfer coefficient of film condensation with the thickness of the falling film and this is commonly taken as a reference to describe filmwise condensation. Other correlations have also been derived from his theory and the current state of the art of filmwise condensation correlations is presented in Table 3.

In order to compare the different pool boiling and condensation correlations and select the most suitable ones, each correlation was compared with the experimental data by considering an overall boiling and condensation heat transfer coefficient. Over the whole range of heat transfer rates (0−1500 W), the average error of the pool boiling and condensation heat transfer coefficient correlation when compared with the experimental heat transfer coefficient is presented in Fig. 7.
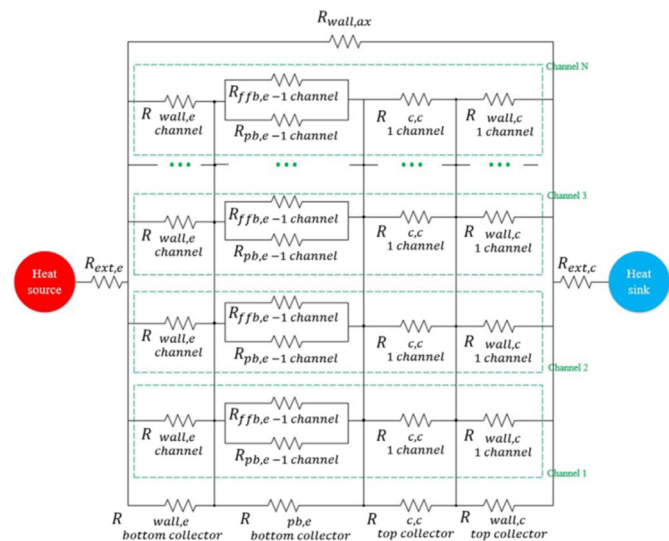

Fig. 6. Multi-channel flat heat pipe thermal resistance model.

Table 2
Nucleate pool boiling heat transfer coefficient h_{nb} correlations.

Authors	Year	Correlation
Kruzhilin [25]	1947	$h_{pb} = 0.082\left(\frac{k_l}{L_b}\right)\left(\frac{i_{lv}q_{pb}''}{gT_{sat}k_l}\frac{\rho_v}{\rho_l - \rho_v}\right)^{0.7}\left(\frac{T_{sat}c_{p,l}\sigma\rho_l}{i_{lv}^2\rho_v^2 L_b}\right)^{0.33}Pr_l^{-0.45}$ where, ❖ $L_b = \left[\frac{\sigma}{g(\rho_l - \rho_v)}\right]^{1/2}$
Rohsenow [22]	1952	$h_{pb} = \left(\frac{q_{pb}''}{i_{lv}}\right)^{1-r}\left[\mu_l / \sqrt{\frac{\sigma}{g(\rho_l - \rho_v)}}\right]^r\frac{c_{p,l}}{C_{sf}}Pr_l^{-s}$ where, ❖ $r = 1/3$ ❖ $\begin{cases} s = n = 1 \text{ for water} \\ s = n = 1.7 \text{ for other fluids} \end{cases}$
McNelly [26]	1953	$h_{pb} = 0.225\left(\frac{q_{pb}''c_p}{i_{lv}}\right)^{0.69}\left(\frac{Pk_l}{\sigma}\right)^{0.31}\left(\frac{\rho_l}{\rho_v} - 1\right)^{0.33}$
Forster and Zuber [27]	1955	$h_{pb} = \frac{0.00122 \times \Delta T_{sat}^{0.24}\Delta P_{sat}^{0.75}c_{p,l}^{0.45}\rho_l^{0.49}k_l^{0.79}}{\sigma^{0.5}i_{lv}^{0.24}\mu_l^{0.29}\rho_v^{0.24}}$
Tien [28]	1962	$h_{pb} = 61.3 k_l Pr_l^{0.33} N_a^{0.5}\Delta T_{sat}$
Lienhard [29]	1963	$h_{pb} = C k_l Pr^{1/3}\frac{\sqrt{\sigma g(\rho_l - \rho_v)/\rho_l^2}\big|_{fluid}}{\sqrt{\sigma g(\rho_l - \rho_v)/\rho_l^2}\big|_{water}}N_a^{1/3}(\Delta T_{sat})^{5/4}$ where, ❖ C is an empirical constant
Mostinskii [30]	1963	$h_{pb} = 3.596 \times 10^{-5}P_{crit}^{0.69}(q_{pb}'')^{0.7}F(P^*)$ where, ❖ $F(P^*) = 1.8P^{*0.17} + 4P^{*1.2} + 10P^{*10}$ ❖ $P^* = P/P_{crit}$
Mikic and Rohsenow [31]	1969	$h_{pb} = 2N_a D_d^2(\pi k_l c_{p,l}\rho_l f_d)^{1/2}$ To estimate the value of bubble related factors N_a, D_d and f_d, authors proposed: ❖ $N_a = r_s^m\left(\frac{i_{lv}\rho_v}{2T\sigma}\right)^m\Delta T_{sat}^m$ ❖ $D_d = a\left[\frac{\sigma}{g(\rho_l - \rho_v)}\right]^{1/2}\left(\frac{\rho_l c_{p,l}T_{sat}}{\rho_v i_{lv}}\right)^{5/4}$ ❖ $f_d = \frac{0.6}{D_d}\left[\frac{\sigma g(\rho_l - \rho_v)}{\rho_v^2}\right]^{1/4}$ ❖ $\begin{cases} a = 1.5 \times 10^{-4} \text{ for water} \\ a = 4.65 \times 10^{-4} \text{ for other fluids} \end{cases}$
Danilova [32]	1970	$h_{pb} = C\left(\frac{R_a}{R_{a0}}\right)^{0.2}(0.14 + 2.2P^*)q_{pb}''^{0.75}$ where, ❖ C is an empirical constant
Labuntsov [33]	1973	$h_{pb} = 0.075\left[1 + 10\left(\frac{\rho_v}{\rho_l - \rho_v}\right)^{0.67}\right]\left(\frac{k_l^2}{\nu_l\sigma T_{sat}}\right)^{0.33}q_{pb}''^{0.67}$
Imura et al. [34]	1979	$h_{pb} = 0.32\left(\frac{\rho_l^{0.65}k_l^{0.3}c_{p,l}^{0.7}g^{0.2}}{\rho_v^{0.25}i_{lv}^{0.4}\mu_l^{0.1}}\right)\left(\frac{P_v}{P_{atm}}\right)^{0.3}q_{pb}''^{0.4}$
Stephan and Preusser [35]	1979	$h_{pb} = 0.1\left(\frac{k_l}{D_d}\right)\left(\frac{q_{pb}''D_d}{k_l T_{sat}}\right)^{0.674}\left(\frac{\rho_v}{\rho_l}\right)^{0.156}\left(\frac{i_{lv}D_d^2}{\alpha_l^2}\right)^{0.371}\left(\frac{\alpha_l^2\rho_l}{\sigma D_d}\right)^{0.35}\left(\frac{\mu_l c_{p,l}}{k_l}\right)^{-0.162}$
Stephan and Abdelsalam [36]	1980	$\begin{cases} h_{pb} = 0.246\frac{k_l}{D_d} \times 10^{-7} \times X_1^{0.673}X_3^{1.26}X_4^{-1.58}X_8^{5.22} \text{ for water} \\ h_{pb} = 0.0546\frac{k_l}{D_d} \times X_1^{0.67}X_4^{0.248}X_5^{1.17}X_8^{-4.33} \text{ for hydrocarbons} \\ h_{pb} = 4.82\frac{k_l}{D_d} \times X_1^{0.624}X_3^{0.374}X_4^{0.329}X_5^{0.257}X_7^{0.117} \text{ for cryogenic fluids} \\ h_{pb} = 207\frac{k_l}{D_d} \times X_1^{0.745}X_5^{0.581}X_6^{0.533} \text{ for refrigerants} \end{cases}$ where, ❖ $X_1 = \left(\frac{q_{pb}''D_d}{k_l T_v}\right)$, $X_2 = \left(\frac{\alpha^2\rho_l}{\sigma D_d}\right)$, $X_3 = \left(\frac{c_p T_v D_d^2}{\alpha^2}\right)$, $X_4 = \left(\frac{i_{lv}D_d^2}{\alpha^2}\right)$ $X_5 = \left(\frac{\rho_v}{\rho_l}\right)$, $X_6 = \left(\frac{c_p\mu_l}{k_l}\right)$, $X_7 = \left(\frac{\rho_{l,w}c_{p,l,w}k_{l,w}}{\rho_l c_{p,l}k_l}\right)$, $X_8 = \left(\frac{\rho_l - \rho_v}{\rho_l}\right)$
Shiraishi et al. [37]	1981	$h_{pb} = 0.32\left(\frac{\rho_l^{0.65}k_l^{0.3}c_{p,l}^{0.7}g^{0.2}}{\rho_v^{0.25}i_{lv}^{0.4}\mu_l^{0.1}}\right)\left(\frac{P_v}{P_{atm}}\right)^{0.23}q_{pb}''^{0.4}$
Bier [38]	1982	$h_{pb} = 3.596 \times 10^{-5}P_{crit}^{0.69}(q_{pb}'')^{0.7}F(P^*)$ where, ❖ $F(P^*) = 0.7 + 2P^*\left(4 + \frac{1}{1 - P^*}\right)$

Table 2 (*continued*)

Authors	Year	Correlation
Nishikawa [39]	1982	$h_{pb} = 31.4 \dfrac{p_{crit}^{0.2}}{M_{mol}^{0.1} T_{crit}^{0.9}} \left(8 \dfrac{R_p}{R_{p0}}\right)^{0.2(1-P^*)} \dfrac{P^{*0.23}}{(1-0.99P^*)^{0.9}} q_{pb}^{\prime\prime 0.8}$
Cooper [40]	1984	$h_{pb} = 55(q_{pb}^{\prime\prime})^{0.67} P^{*(0.12-0.2\log R_{a,p})} (-\log P^*)^{-0.55} M_{mol}^{-1/2}$
Ueda et al. [41]	1988	$h_{pb} = C_{sf}^{-1} Pr_l^{-1.7} \left(\dfrac{c_{p,l}}{i_{lv}} q_{pb}^{\prime\prime}\right) \left(\dfrac{L_b}{i_{lv}\mu_l} q_{pb}^{\prime\prime}\right)^{-1/3}$ where, ❖ $L_b = \left[\dfrac{\sigma}{g(\rho_l - \rho_v)}\right]^{1/2}$ ❖ $\begin{cases} C_{sf} = 0.0098 \text{ for water} \\ C_{sf} = 0.0028 \text{ for methanol} \\ C_{sf} = 0.0047 \text{ for } R-113 \end{cases}$
Kutateladze [42]	1990	$h_{pb} = 0.44 Pr_l^{0.35} \left(\dfrac{k_l}{L_b}\right) \left(\dfrac{\rho_l}{\rho_l - \rho_v} \dfrac{P \times 10^{-4}}{\rho_v g i_{lv} \mu_l} q_{pb}^{\prime\prime}\right)^{0.7}$ where, ❖ $L_b = \left[\dfrac{\sigma}{g(\rho_l - \rho_v)}\right]^{1/2}$
Kutateladze (new)	1990	$h_{pb} = \left[3.37 \times 10^{-9} \dfrac{k_l}{L_b} \left(\dfrac{q_{pb}^{\prime\prime} c_{p,l}}{i_{lv}}\right)^2 M_*^{-4}\right]^{\frac{1}{3}}$ where, ❖ $L_b = \left[\dfrac{\sigma}{g(\rho_l - \rho_v)}\right]^{1/2}$ ❖ $M_*^{-4} = \dfrac{(P/\rho_v)^2}{\sigma g/(\rho_l - \rho_v)}$
Groβ [43]	1990	$h_{pb} = 55 q_{pb}^{\prime\prime 0.7} [P^{*0.12}/((-\log_{10} P^*)^{0.55} \sqrt{M_{mol}})]$
Gorenflo et al. [44]	1990	$h_{pb} = h_o F(P^*)(q_{pb}^{\prime\prime}/q_0^{\prime\prime})^n (R_a/R_{a0})^{0.133}$ where, ❖ $\begin{cases} F(P^*) = 1.73 P^{*0.27} + \left(6.1 + \dfrac{0.68}{1-P^*}\right) P^{*2} \text{ for water} \\ F(P^*) = 1.2 P^{*0.27} + 2.5 P^* + \dfrac{P^*}{1-P^*} \text{ for all other fluids except liquid helium} \end{cases}$ ❖ $\begin{cases} n = 0.9 - 0.3 P^{*0.15} \text{ for water} \\ n = 0.9 - 0.3 P^{*0.3} \text{ for all other fluids except liquid helium} \end{cases}$
Kaminaga et al. [45]	1992	$h_{pb} = 22(\rho_v/\rho_l)^{0.4} R_{a,p}^{0.2(1-P^*)} h_{pb,Kutateladze}$ where, $h_{pb,Kutateladze} = 0.44 Pr_l^{0.35} \left(\dfrac{k_l}{L_b}\right) \left(\dfrac{\rho_l}{\rho_l - \rho_v} \dfrac{P \times 10^{-4}}{\rho_v g i_{lv} \mu_l} q_{pb}^{\prime\prime}\right)^{0.7}$
Leiner [46], *Leiner and Gorenflo* [47]	1994	$h_{pb}^* = A F'(P^*) q^{*n} R^{*0.133}$ where, ❖ $h_{pb}^* = \dfrac{h_{pb}}{P_{crit}(R_{mol}/M_{mol}T_{crit})^{1/2}}$ ❖ $q^* = \dfrac{q_{pb}^{\prime\prime}}{P_{crit}(R_{mol}T_{crit}/M_{mol})^{1/2}}$ ❖ $R^* = \dfrac{R_a}{(R_{mol}T_{crit}/P_{crit}N_{mol})^{1/3}}$ ❖ $F'(P^*) = 43000^{(n-0.75)} \left[1.2 P^{*0.27} + \left(2.5 + \dfrac{1}{1-P^*}\right) P^*\right]$ ❖ $\begin{cases} n = 0.9 - 0.3 P^{*0.15} \text{ for water} \\ n = 0.9 - 0.3 P^{*0.3} \text{ for all other fluids except liquid helium} \end{cases}$ ❖ $A = 0.6161 C^{0.1512} K^{0.4894}$ ❖ $C = \dfrac{c_{p,l}|_{P^*=0.1}}{R}$ ❖ $K = \dfrac{T_{crit} \ln(P^*)}{(1-T_{crit})}$
Chowdhury et al. [48]	1997	$\begin{cases} h_{pb} = 11.43(Re_b)^{0.72}(Pr_l)^{0.42} \left(\dfrac{\rho_v}{\rho_l}\right)^{0.5} \left(\dfrac{D_d}{D_i}\right) \left(\dfrac{k_l}{D_d}\right) \text{ for water} \\ h_{pb} = 495.7(Re_b)^{0.8}(Pr_l)^{0.5} \left(\dfrac{\rho_v}{\rho_l}\right)^{0.33} \left(\dfrac{k_l}{D_d}\right) \text{ for ethanol} \\ h_{pb} = 6(Re_b)^{0.78}(Pr_l)^{0.48} \left(\dfrac{\rho_v}{\rho_l}\right)^{0.58} \left(\dfrac{k_l}{D_d}\right) \text{ for Freon } R-113 \end{cases}$ where, ❖ $Re_b = \dfrac{q_{pb}^{\prime\prime} D_d}{\rho_v i_{lv} \nu_l}$
El-Genk and Saber [49]	1998	

Table 2 (*continued*)

Authors	Year	Correlation
Kiatsiriroat et al. [50]	2000	$h_{pb} = (1 + 4.95\psi) \times h_{pb,Kutateladze}$ where, ❖ $h_{pb,Kutateladze} = 0.44 Pr_l^{0.35} \left(\frac{k_l}{L_b}\right)\left(\frac{\rho_l}{\rho_l - \rho_v}\frac{P \times 10^{-4}}{\rho_v g i_{lv}\mu_l}q''_{pb}\right)^{0.7}$ ❖ $\psi = \left(\frac{\rho_v}{\rho_l}\right)^{0.4}\left[\frac{P_v\nu_l}{\sigma}\left(\frac{\rho_l^2}{\sigma g(\rho_l - \rho_v)}\right)^{1/4}\right]^{1/4}$ ❖ $L_b = \left[\frac{\sigma}{g(\rho_l - \rho_v)}\right]^{1/2}$ $h_{pb} = C\left(\frac{\mu i_{lv}}{L_b \Delta T_{sat}}\right)\left(\frac{c_p \Delta T_{sat}}{i_{lv}Pr}\right)^{3n}$ where, ❖ $L_b = \left[\frac{\sigma}{g(\rho_l - \rho_v)}\right]^{1/2}$ ❖ $\begin{cases} C = 18.688 \text{ for water} \\ C = 17.625 \text{ for ethanol} \\ C = 20.565 \text{ for triethylene glycol (TEG)} \end{cases}$ ❖ $\begin{cases} n = 0.3572 \text{ for water} \\ n = 0.3300 \text{ for ethanol} \\ n = 0.3662 \text{ for triethylene glycol (TEG)} \end{cases}$
Ribatski and Jabardo [51]	2003	$h_{pb} = C\left(\frac{R_a}{R_{a0}}\right)^{0.2}P^{*0.45}[-\log(P^*)]^{-0.8}M_{mol}^{-0.5}q''^n_{pb}$ where, ❖ $\begin{cases} C = 100 \text{ for copper} \\ C = 110 \text{ for brass} \\ C = 85 \text{ for stainless steel} \end{cases}$ ❖ $n = 0.9 - 0.3P^{*0.2}$

Based on the experimental heat transfer coefficient measured, the best performing pool boiling correlations were found to be the correlation by *Rohsenow* [22] with an average error of 12.8% and the correlation by *Stephan and Preusser* [35] with an average error of 12.7%. Other correlations such as the correlations by *El-Genk and Saber* [49], *Stephan and Abdelsalam* [36], and *Gorenflo* et al. [44] also performed well but showed a lower accuracy on average. As for condensation, the correlation by *Hussein* et al. [59] clearly stands out. For the overall range of heat transfer rate, the average error of this correlation was found to be 15.1%. Hence, the correlations by *Rohsenow* [22] and *Hussein* et al. [59] were selected for integration in the proposed multi-channel flat heat pipe thermal resistance model.

An iterative model was built using Excel with macros and VBA coding based on the multi-channel heat pipe thermal resistance network proposed and the two-phase heat transfer coefficient correlations selected. In this model, iterations are conducted for two purposes. At first, iterations are needed to calculate the boiling and condensation thermal resistances that depend on the wall temperatures. Second, the temperature of the heat pipe evaporator and of all the temperatures in the heat pipe are adjusted by the model until an energy balance is reached. This energy balance relates the heat transfer rate measured through the system to the heat transfer rate that can be extracted by the cooling manifold. According to the first law of thermodynamics, the energy that passes through the system and recovered by the cooling water circulating inside the cooling manifold is given by:

$$\dot{Q}_{provided} = \dot{m}_{water}c_{p,water}\Delta T_{water} \tag{16}$$

where $\dot{Q}$ is the heat transfer rate through the system (W), $\dot{m}_{water}$ is the water flow rate in the cooling manifold (kg/s), $c_{p,water}$ is the specific heat of water (J/kg.K), and ΔT_{water} is the temperature difference in the water flow (K). When estimating the temperatures of the system, the iterative tool adjusts the evaporator temperature of the multi-channel heat pipe and, based on the thermal resistance network proposed, calculates the temperature everywhere in the

system. In so doing, the surface temperature in contact with the manifold is predicted and the energy extracted from this surface by the cooling manifold is obtained from:

$$\dot{Q}_{calculated} = \frac{1}{R_{manifold}} \times \frac{T_{water-in} - T_{water-out}}{ln((T_s - T_{water-out})/(T_s - T_{water-in}))} \tag{17}$$

where $\dot{Q}_{calculated}$ is the calculated heat transfer rate at each iteration based on the system temperature (W), $R_{manifold}$ is the cooling manifold thermal resistance (K/W), $T_{water-in}$ and $T_{water-out}$ are the water inlet and outlet temperatures (K), and T_s is the surface temperature of the heat pipe in contact with the cooling manifold (K). The model changes the evaporator temperature of the flat heat pipe using the log mean temperature difference equation described in Eq. (17), until the temperature at the heat pipe and cooling manifold interface permits the target heat transfer rate to be extracted. The iterations stop when the following criterion is reached (within 0.1%):

$$\dot{Q}_{calculated} = \dot{Q}_{provided} \tag{18}$$

6. Results

6.1. Impact of the heat transfer rate on the thermal performance of the multi-channel flat heat pipe and theoretical model validation

In this section, the multi-channel flat heat pipe is kept in a vertical position and the heat transfer rate is varied in the range 0–1500 W. The experimental heat transfer rate is taken as the heat dissipated by the water flow which is equal to the heat provided by the heat source minus small thermal losses (around 10–20 W). Fig. 8 presents the impact of the heat transfer rate on the boiling thermal resistance of the multi-channel flat heat pipe. In Fig. 8, the black circles represent the experimental data whereas the

Table 3
Filmwise condensation heat transfer coefficient h_c correlations.

Author	Year	Correlation
Laminar falling film ($\textbf{Re}_f \leq 20-30$) **and Wavy-laminar falling film** ($20-30 \leq \textbf{Re}_f \leq 600$)		
Nusselt [23]	1916	$h_{Nusselt} = 0.943 \left\{ \frac{\rho_l(\rho_l - \rho_v)i_{lv}gk_l^3}{\mu_l L_c(T_{sat} - T_w)} \right\}^{1/4}$
McAdams [52]	1942	$h_c = 1.13 \left\{ \frac{\rho_l(\rho_l - \rho_v)i_{lv}gk_l^3}{\mu_l L_c(T_{sat} - T_w)} \right\}^{1/4}$
Nusselt [23] corrected by *Rohsenow* [53]	1956	$h_c = 0.943 \left\{ \frac{\rho_l(\rho_l - \rho_v)i_{lv}'gk_l^3}{\mu_l L_c(T_{sat} - T_w)} \right\}^{1/4}$ where, ❖ Correction for a subcooled condensate: $i_{lv}' = i_{lv} + {}^3/_8 c_{pl}(T_{sat} - T_w)$ ❖ Correction for a non-linear temperature distribution: $i_{lv}' = i_{lv} + 0.68 c_{pl}(T_{sat} - T_w)$ ❖ Correction for a shear-stress dominating flow, linear temperature distribution and potential subcooling of the condensate: $i_{lv}' = i_{lv} + {}^1/_3 c_{pl}(T_{sat} - T_w)$ ❖ Correction in the case where both gravity and shear stress are significant: $h_c = (h_{correction:non-linear\ temperature}^2 + h_{correction:shearstress}^2)^{1/2}$
Rohsenow [53]	1956	$h_c = 1.51 \left(\frac{P_v}{P_{crit}} \right)^{0.14} \times 0.943 \left\{ \frac{\rho_l(\rho_l - \rho_v)gk_l^3}{\mu_l L_c(T_{sat} - T_w)} \left[i_{lv} + {}^3/_8 c_{pl}(T_{sat} - T_w) \right] \right\}^{1/4}$ where the fluid properties should be evaluated at a temperature: $T = T_W + 0.31(T_{sat} - T_w)$
Kutateladze (old) [54]	1963	$h_c = 0.69 Re_{f,L_c}^{0.11} \times h_{Nusselt}$ where, ❖ $Re_{f,L_c} = \frac{4\Gamma_{L_c}}{\mu_l}$
Kutateladze (new) [54]	1963	$h_c = \frac{Re_{f,L_c}/4}{1.47(Re_{f,L_c}/4)^{1.22} - 1.3} k_l \left(\frac{\mu_l^2}{\rho_l(\rho_l - \rho_v)g} \right)^{-1/3}$ where, ❖ $Re_{f,L_c} = \frac{4\Gamma_{L_c}}{\mu_l}$
Butterworth [55]	1981	$h_c = 1.013 Re_{f,L_c}^{-0.22} k_l \left(\frac{\mu_l^2}{\rho_l(\rho_l - \rho_v)g} \right)^{-1/3}$ where, ❖ $Re_{f,L_c} = \frac{4\Gamma_{L_c}}{\mu_l}$
Wang and Ma [56]	1991	$h_c = \left(\frac{L_c}{r_i} \right)^{\frac{\cos(\beta)}{4}} [0.54 + (5.68 \times 10^{-3}\beta)]h_{Nusselt}$ where, ❖ β: Inclination angle of the thermosyphon (°) ❖ L_c: Condenser length (m) ❖ r_i: Internal radius of the thermosyphon (m)
Gross [57]	1998	$h_c = ((0.925 f_d Re_{f,max}^{-1/3})^2 + (0.044 Pr_l^{2/5} Re_{f,max}^{1/6})^2)^{1/2} k_l \left(\frac{\mu_l^2}{\rho_l(\rho_l - \rho_v)g} \right)^{-1/3}$ where, ❖ $f_d = (1 - 0.63(P_v/P_{crit})^{3.3})^{-1}$ ❖ $Re_{f,max} = Re_f = \frac{q}{\pi D_i i_{lv} \mu_l}$
Schnabel and Palen [58]	1998	$h_c = 0.693 \left(\frac{1 - \rho_v/\rho_l}{Re_f/4} \right)^{1/3} k_l \left(\frac{\mu_l^2}{\rho_l(\rho_l - \rho_v)g} \right)^{-1/3}$ where, ❖ $Re_f = 4\Gamma/\mu_l$
Hussein et al. [59]	2001	$h_c = \left(\frac{L_c}{D_i} \right)^{\frac{1}{4}(\cos(\beta))^{0.358}} [0.997 - 0.334(\cos(\beta))^{0.108}]h_{Nusselt}$ where, ❖ β: Inclination angle of the thermosyphon (°) ❖ L_c: Condenser length (m) ❖ D_i: Internal diameter of the thermosyphon (m)
Fiedler and Auracher [60]	2004	$h_c = \left(\frac{L_c}{r_i} \right)^{\cos(\beta/4)} [0.125 + (1.46 \times 10^{-2}\beta) - (7.27 \times 10^{-5}\beta^2)]h_{Nusselt}$ where, ❖ β: Inclination angle of the thermosyphon (°) ❖ L_c: Condenser length (m) ❖ r_i: Internal radius of the thermosyphon (m)
Wavy falling film ($600 \leq \textbf{Re}_f \leq 1600$)		
Kutateladze (old) [54]	1963	$h_c = 0.69 Re_{f,L_c}^{0.11} \times h_{Nusselt}$ where,

Table 3 (*continued*)

Author	Year	Correlation
Kutateladze (new) [54]	1963	❖ $Re_{f,L_c} = \dfrac{4\Gamma_{L_c}}{\mu_l}$ $h_c = \dfrac{Re_{f,L_c}/4}{1.47(Re_{f,L_c}/4)^{1.22} - 1.3} k_l \left(\dfrac{\mu_l^2}{\rho_l(\rho_l - \rho_v)g} \right)^{-1/3}$ where,
Butterworth [55]	1981	❖ $Re_{f,L_c} = \dfrac{4\Gamma_{L_c}}{\mu_l}$ $h_c = 1.013 Re_{f,L_c}^{-0.22} k_l \left(\dfrac{\mu_l^2}{\rho_l(\rho_l - \rho_v)g} \right)^{-1/3}$ where,
Uehara et al. [61]	1983	❖ $Re_{f,L_c} = \dfrac{4\Gamma_{L_c}}{\mu_l}$ $h_c = 1.013 Re_{f,\beta}^{-1/3} k_l \left(\dfrac{\mu_l^2}{\rho_l(\rho_l - \rho_v)g} \right)^{-1/3}$ where, ❖ $Re_{f,\varphi} = \dfrac{q}{\pi D_i i_{lv}\mu_l} \times f_\beta$ ❖ $\begin{cases} f_\beta = 1 \text{ for vertical tube} \\ f_\beta = 2.87\left(\dfrac{D_i}{L_c \sin(\beta)}\right) \text{ for inclined tube with } 10° < \beta \end{cases}$
Chun and Kim [62]	1991	$h_c = [1.33 Re_{f,L_c}^{-1/3} + 9.56 \times 10^{-6} Re_{f,L_c}^{0.89} Pr_l^{0.94} + 8.22 \times 10^{-2}] k_l \left(\dfrac{\mu_l^2}{\rho_l(\rho_l - \rho_v)g} \right)^{-1/3}$ where, ❖ $Re_{f,L_c} = \dfrac{4\Gamma_{L_c}}{\mu_l}$
Gross [57]	1992	$h_c = ((0.925 f_d Re_{f,max}^{-1/3})^2 + (0.044 Pr_l^{2/5} Re_{f,max}^{1/6})^2)^{1/2} k_l \left(\dfrac{\mu_l^2}{\rho_l(\rho_l - \rho_v)g} \right)^{-1/3}$ where, ❖ $f_d = (1 - 0.63(P_v/P_{crit})^{3.3})^{-1}$ ❖ $Re_{f,max} = Re_f = \dfrac{q}{\pi D i_{lv}\mu_l}$
Nozhat [63]	1995	$h_c = 0.87 Re_{f,L_c}^{0.07} \times h_{Nusselt}$ where, ❖ $Re_{f,L_c} = \dfrac{4\Gamma_{L_c}}{\mu_l}$
Schnabel and Palen [58]	1998	$h_c = (h_{laminar}^2 + h_{turbulent}^2)^{1/2}$ $h_{laminar} = 0.693 \left(\dfrac{1 - \rho_v/\rho_l}{Re_f/4} \right)^{1/3} k_l \left(\dfrac{\mu_l^2}{\rho_l(\rho_l - \rho_v)g} \right)^{-1/3}$ $h_{turbulent} = \dfrac{0.0283(Re_f/4)^{7/24} Pr_l^{1/3}}{1 + 9.66(Re_f/4)^{-3/8} Pr_l^{-1/6}} k_l \left(\dfrac{\mu_l^2}{\rho_l(\rho_l - \rho_v)g} \right)^{-1/3}$ where, ❖ $Re_f = 4\Gamma/\mu_l$
Hashimoto and Kaminaga [64]	2002	$h_c = 0.85 Re_f^{0.1} exp\left(-6.7 \times 10^{-5}\dfrac{\rho_l}{\rho_v} - 0.6 \right) h_{Nusselt}$ where, ❖ $Re_f = 4\Gamma/\mu_l$
Jouhara and Robinson [65]	2010	$h_c = 0.85 Re_f^{0.1} exp\left(-6.7 \times 10^{-5}\dfrac{\rho_l}{\rho_v} - 0.14 \right) h_{Nusselt}$ where, ❖ $Re_f = \dfrac{4q}{\pi D_i i_{lv}\mu_l}$
Turbulent falling film ($1600 \leq Re_f \leq 3200$) **and Highly turbulent falling film** ($3200 \leq Re_f$)		
Labuntsov [66]	1957	$h_c = 0.0306 Re_{f,L_c}^{1/4} Pr_l^{1/2} k_l \left(\dfrac{\mu_l^2}{\rho_l(\rho_l - \rho_v)g} \right)^{-1/3}$ where, ❖ $Re_{f,L_c} = \dfrac{4\Gamma_{L_c}}{\mu_l}$
Uehara et al. [61]	1983	$h_c = 0.044 Pr_l^{2/5} Re_{f,\beta}^{1/6} k_l \left(\dfrac{\mu_l^2}{\rho_l(\rho_l - \rho_v)g} \right)^{-1/3}$ where, ❖ $Re_{f,\varphi} = \dfrac{q}{\pi D_i i_{lv}\mu_l} \times f_\beta$ ❖ $\begin{cases} f_\beta = 1 \text{ for vertical tube} \\ f_\beta = 2.87\left(\dfrac{D_i}{L_c \sin(\beta)}\right) \text{ for inclined tube with } 10° < \beta \end{cases}$
Chun and Kim [62]	1991	$h_c = [1.33 Re_{f,L_c}^{-1/3} + 9.56 \times 10^{-6} Re_{f,L_c}^{0.89} Pr_l^{0.94} + 8.22 \times 10^{-2}] k_l \left(\dfrac{\mu_l^2}{\rho_l(\rho_l - \rho_v)g} \right)^{-1/3}$ where, ❖ $Re_{f,L_c} = \dfrac{4\Gamma_{L_c}}{\mu_l}$

Table 3 (continued)

Author	Year	Correlation
Gross [57]	1992	$h_c = ((0.925f_d Re_{f,max}^{-1/3})^2 + (0.044Pr_l^{2/5}Re_{f,max}^{1/6})^2)^{1/2} k_l \left(\frac{\mu_l^2}{\rho_l(\rho_l - \rho_v)g}\right)^{-1/3}$ where, ❖ $f_d = (1 - 0.63(P_v/P_{crit})^{3.3})^{-1}$ ❖ $Re_{f,max} = Re_f = \frac{q}{\pi D i_{lv}\mu_l}$
Schnabel and Palen [58]	1998	$h_c = \frac{0.0283(Re_f/4)^{7/24}Pr_l^{1/3}}{1 + 9.66(Re_f/4)^{-3/8}Pr_l^{-1/6}} k_l \left(\frac{\mu_l^2}{\rho_l(\rho_l - \rho_v)g}\right)^{-1/3}$ where, ❖ $Re_f = 4\Gamma/\mu_l$
Hashimoto and Kaminaga [64]	2002	$h_c = 0.85Re_f^{0.1}exp\left(- 6.7 \times 10^{-5}\frac{\rho_l}{\rho_v} - 0.6\right)h_{Nusselt}$ where, ❖ $Re_f = \frac{4q}{\pi D_i i_{lv}\mu_l}$
Jouhara and Robinson [65]	2010	$h_c = 0.85Re_f^{0.1}exp\left(- 6.7 \times 10^{-5}\frac{\rho_l}{\rho_v} - 0.14\right)h_{Nusselt}$ where, ❖ $Re_f = \frac{4q}{\pi D_i i_{lv}\mu_l}$

theoretical predictions from the multi-channel model are shown with red crosses.

At heat transfer rates in the range 0–1500 W, the boiling thermal resistance keeps decreasing. At heat transfer rates lower than 400 W, it is noted that the boiling thermal resistance of the multi-channel flat heat pipe is significantly higher due to a moderated boiling activity. In this range of heat transfer rates, the boiling regime mainly belongs to the natural convection boiling regime [20] which produces less turbulent boiling activity and thus a slightly lower heat transfer coefficient. With an increase of the heat transfer rate, the boiling activity increases which leads to a better mixing in the liquid pool and results in a rapid increase in the pool boiling heat transfer coefficient. As a result, the experimental pool boiling thermal resistance decreases from 0.005 K/W at 100 W to 0.0025 K/W at 400 W. At heat transfer rates higher than 400 W, the boiling thermal resistance of the multi-channel flat heat pipe decreases with a linear trend. At a maximum heat transfer rate of 1500 W, the boiling thermal resistance of the heat pipe is at a minimum and down to 0.001 K/W.

Concerning the model prediction of the boiling thermal resistance of the multi-channel flat heat pipe, the theoretical boiling thermal resistance is higher than the experimental data at low heat transfer rates and the prediction is less accurate. With an increase of the heat transfer rate, the error made by the theoretical model
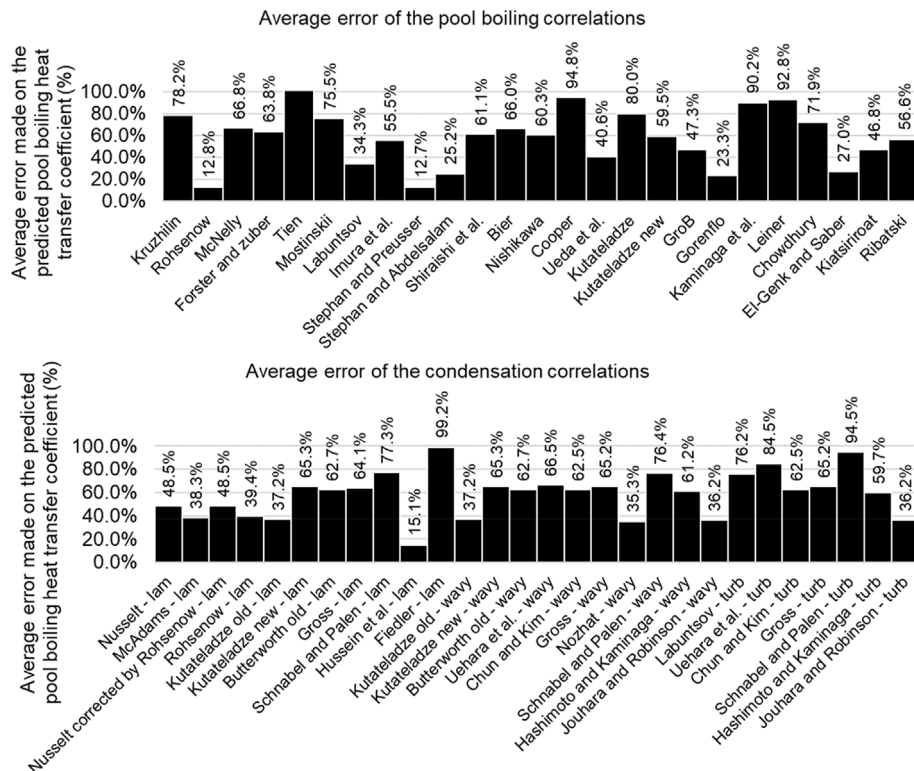

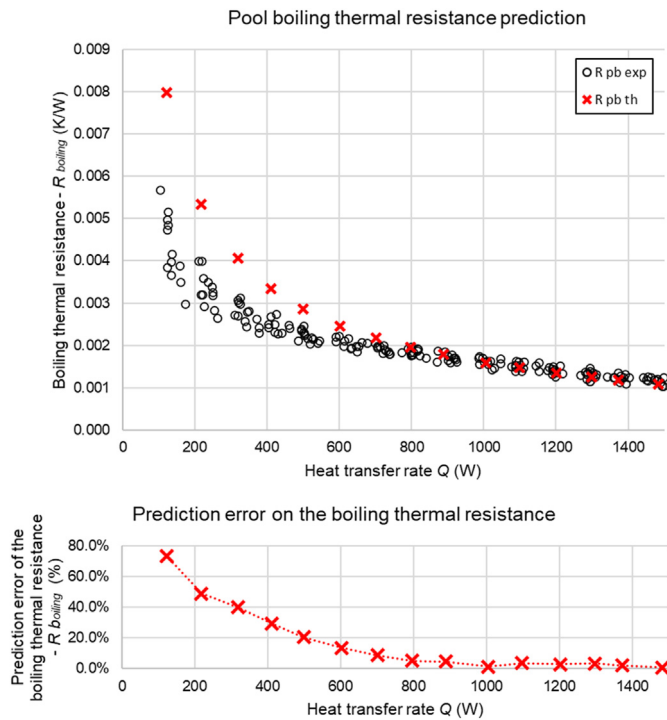**Fig. 7.** Average error of the pool boiling and condensation correlations.

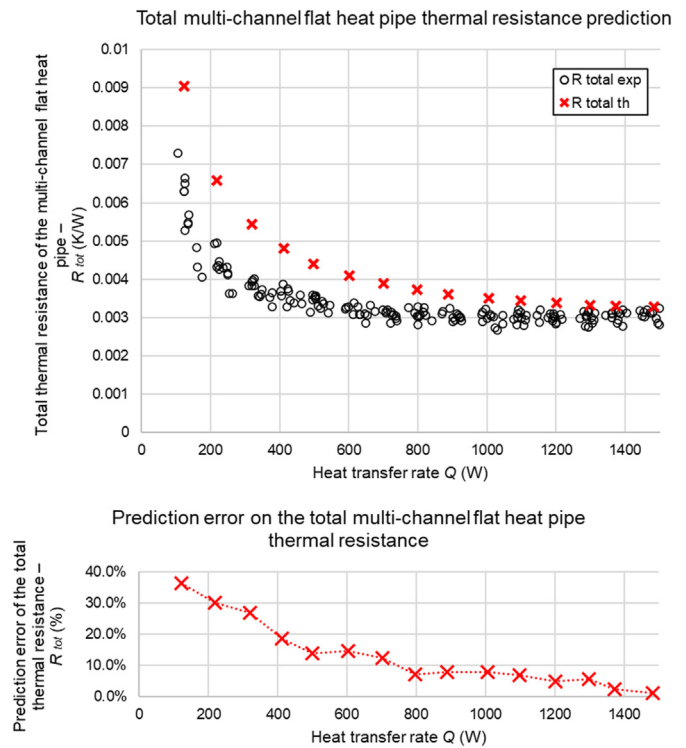**Fig. 8.** Pool boiling thermal resistance prediction.

Fig. 9. Condensation thermal resistance prediction.

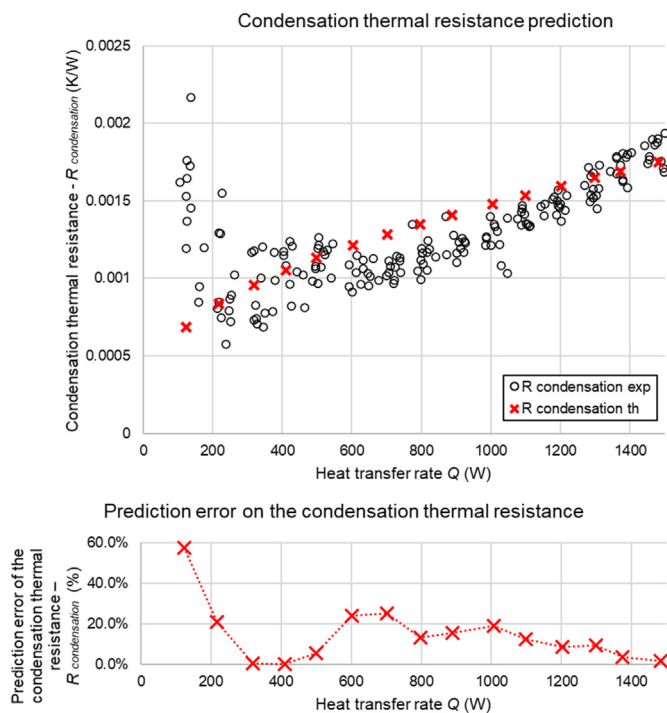**Fig. 10.** Total multi-channel flat heat pipe thermal resistance prediction.

heat transfer range, the average error made by the proposed multi-channel flat heat pipe model on the pool boiling resistance prediction is 17.2%.

Fig. 9 presents the impact of the heat transfer rate on the condensation thermal resistance of the multi-channel flat heat pipe.

As for the condensation, it is observed that the condensation thermal resistance first decreases at low heat transfer rates and then progressively increases. This evolution is linked to the increase of the condensate thickness due to a higher mass transfer rate at higher heat transfer rates. At low heat transfer rates, the increase of the condensation thermal resistance is expected to be caused by the start-up of the heat pipe, and this phenomenon is not predicted by the theoretical model. From 100 W to 400 W, the condensation thermal resistance of the heat pipe decreases from 0.0017 K/W to 0.001 K/W. With the increase of the condensate film thickness, the thermal resistance increases from 0.001 K/W at 400 W to almost 0.002 K/W at 1500 W.

With the observed increased condensation thermal resistance of the multi-channel flat heat pipe at low heat transfer rates, at 100 W, the prediction error is at a maximum due to an over prediction of the heat transfer coefficient. However, from 200 W, the model predicts the condensation thermal resistance of the multi-channel heat pipe within a 30% error. While the model underpredicts the condensation thermal resistance before 400 W, it tends to slightly overestimate this value beyond 400 W. At 400 W, the prediction curve crosses the experimental curve which leads to errors close to 0%. At high heat transfer rates, it is again observed that the multi-channel model proposed becomes more accurate. On the overall range of heat transfer rates studied, the agreement between the model and the condensation experimental data leads to an average error of 14.4%.

The predicted errors made on the total multi-channel flat heat pipe at heat transfer rates in the range 0−1500 W are presented in

decreases and, from a heat transfer rate of 400 W, the pool boiling resistance prediction error is lower than 30%. The accuracy of the proposed model regarding the boiling thermal resistance of the multi-channel flat heat pipe becomes very high at high heat transfer rates and, from a heat transfer rate of 700 W, the error made by the theoretical model is lower than 10%. On the overall

Fig. 10.

Due to the transition from natural convection boiling to the fully developed nucleate boiling regime, the thermal resistance of the multi-channel flat heat pipe is higher at low heat transfer rates and decreases from 0.007 K/W at 100 W to 0.0035 K/W at 400 W. At higher heat transfer rates, the thermal resistance of the multi-channel flat heat pipe stabilizes at around 0.003 K/W. This is due to two phenomena compensating: on the one side, the boiling thermal resistance decreases progressively with the increase in boiling activity whereas, on the other side, the condensation thermal resistance increases with the increase in the film condensate thickness.

It is observed that the multi-channel heat pipe model tends to over-predict the thermal resistance of the multi-channel flat heat pipe. With an increase of the heat transfer rate, the accuracy of the model is improved. Overall, an average error of 13.1% for the proposed multi-channel flat heat pipe is reached.

To bring some perspective about the theoretical model proposed, a comparison with existing models of multi-channel heat pipes is relevant. As previously introduced, only two models available in the literature are reported to predict the thermal performance of a multi-channel heat pipe and were developed by *Almahmoud and Jouhara* [15,16] and *Delpech* et al. [17]. Those two existing models are similar than the presented model in terms of calculation process and their complexities are close. *Almahmoud and Jouhara* [15,16] and *Delpech* et al. [17] used radiation as a heat source which made the radiation model more complex than the current model where electric heaters were used. However, the heat pipe model itself is close to the current model and uses iterations to determine each thermal resistance of the heat pipe thermal resistance network. As a novelty, the proposed model considers different thermal resistances for each parallel channel and for both top and collectors whereas *Almahmoud and Jouhara* [15,16] and *Delpech* et al. [17] considered only one thermal resistance for boiling and condensation with an equivalent heat transfer area. In

terms of prediction accuracy, for heat transfer rates between 4500 W and 8500 W, *Almahmoud and Jouhara* [15,16] predicted the heat transfer rate with 14.3% of error and the heat pipe temperatures were predicted within 3 °C. *Delpech* et al. [17] have reached a better accuracy and predicted the heat transfer rate within 7.5% but at heat transfer rates in the range 470 W−2435 W. Unfortunately, the heat pipe thermal resistance prediction accuracy wasn't clearly reported but the boiling and condensation resistances were predicted within ±25%. As a comparison, the proposed model didn't focus on the heat transfer rate prediction but instead predicted the boiling and condensation thermal resistances inside the heat pipe at a given heat transfer rate. In a range 100 W−1500 W, the average error on the boiling and condensation thermal resistances prediction is 17.2% and 14.4%. It seems that the prediction accuracy for the boiling and condensation thermal resistances of the current model is comparable to that of *Delpech* et al. [17] and seems to be highly related to the two-phase correlations used.

6.2. Impact of the tilt angle on the thermal performance of the multi-channel flat heat pipe

In this section, the tilt angle of the heat pipe was changed and its impact on the thermal resistances of the multi-channel flat heat pipe is studied. The different tilt angles investigated are 90° (vertical), 45°, 20°, 10°, 5°, and 2°. During the experiments, it was observed that the impact of the tilt angle varied with the heat transfer rate. The heat transfer rate was again varied from 100 W to 1500 W. Fig. 11 presents the impact of the tilt angle on the boiling thermal resistance of the multi-channel flat heat pipe at various heat transfer rates.

In Fig. 11, each heat transfer rate at which the impact of the tilt angle is investigated is represented by a single curve with a different colour. One can observe that the impact of the tilt angle on the boiling thermal resistance of the multi-channel flat heat pipe differs significantly with the heat transfer rate. At low heat transfer rates, large variations are observed whereas the impact of the tilt
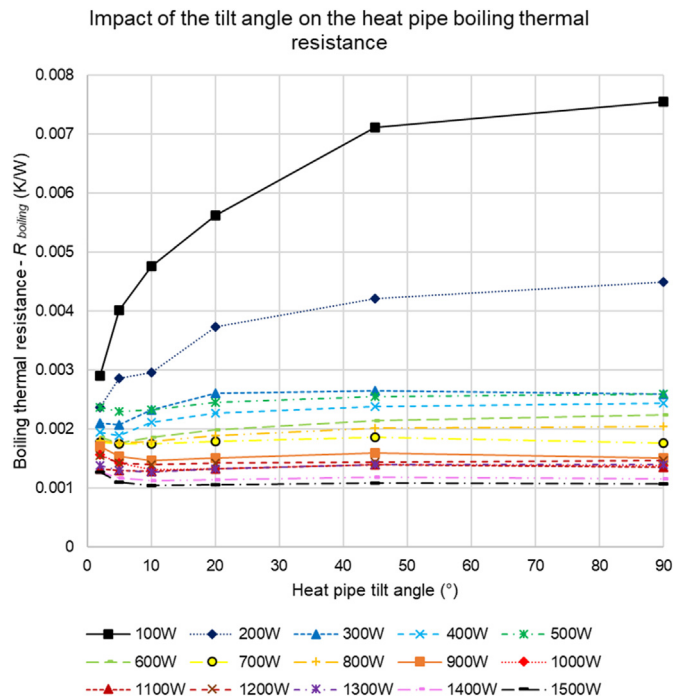

Fig. 11. Impact of the tilt angle on the multi-channel flat heat pipe boiling thermal resistance.
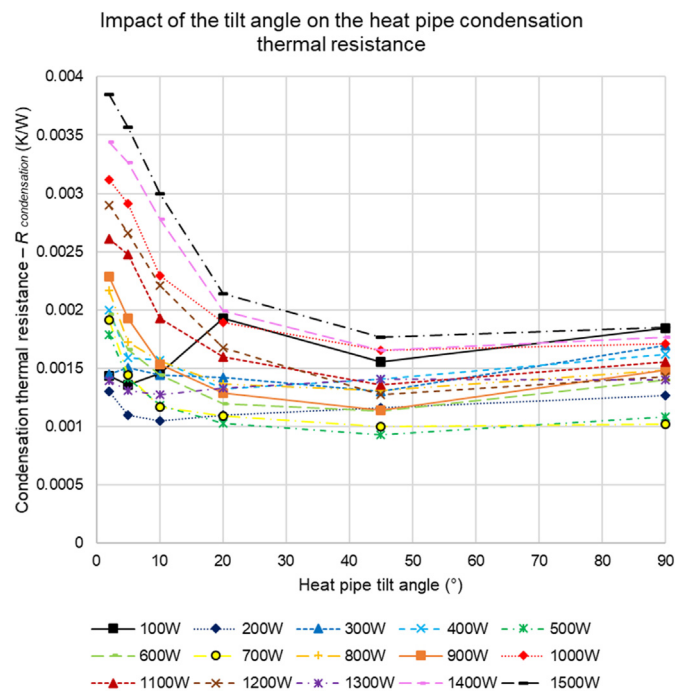

Fig. 12. Impact of the tilt angle on the multi-channel flat heat pipe condensation thermal resistance.

angle becomes less significant at high heat transfer rates. At 100 W, the boiling thermal resistance varies by 0.0046 K/W whereas it varies only by 0.0002 K/W at 1500 W when changing the tilt angle. At heat transfer rates of 100 W and 200 W, the measured boiling thermal resistance of the heat pipe is at a minimum at angles close to the horizontal (2°) and increases when the heat pipe is rotated to a vertical position. The trend is similar to a logarithm function with a fast increase of the boiling thermal resistance at low tilt angles which progressively stabilizes up to the vertical position. With an increase of the heat transfer rate and of the boiling activity, the impact of the tilt angle reduces rapidly. Hence, it seems that the tilt angle of the heat pipe has a significant impact during the natural convection boiling regime. From a heat transfer rate of 300 W, the boiling thermal resistance of the multi-channel flat heat pipe remains fairly similar at tilt angles higher than 20°. Interestingly, at tilt angles lower than 10°, small variations of the boiling thermal resistance are observed. At heat transfer rates in the range 300 W−700 W, when decreasing the tilt angle from 10° to 2°, the boiling thermal resistance decreases slightly by 0.0001 K/W. The opposite phenomenon is observed at heat transfer rates in the range 800 W−1500 W where the thermal resistance increases slightly by 0.0002 K/W at the same tilt angles. With tilt angles very close to the horizontal, it is concluded that the increase of the pool boiling heat transfer area leads to a similar boiling pattern at the bottom of the channels, independent of the heat transfer rate. At higher tilt angles, the impact on the boiling thermal resistance depends on the heat transfer rate and boiling activity. The higher the heat transfer rate and boiling activity, the smaller the impact of the tilt angle on the boiling thermal resistance of the multi-channel flat heat pipe.

Fig. 12 studies the impact of the tilt angle on the condensation thermal resistance.

In contrast with the impact of the tilt angle on the boiling thermal resistance, the condensation thermal resistance of the multi-channel flat heat pipe is more affected, when increasing the heat transfer rate. Due to experimental inaccuracies, the curve for a heat transfer rate of 100 W shows a significant discontinuity and it is considered inaccurate. Hence, to characterize the impact of the tilt angle on the condensation thermal resistance at low heat transfer rates, the evolutions at 200 W and 300 W are given greater weight. At low heat transfer rates in the range 100 W−300 W, the condensation thermal resistance mainly varies at tilt angles less than 10°. A small increase in the condensation thermal resistance is observed, when getting close to the horizontal position. Only a very small increase in the condensation thermal resistance can be seen from a tilt angle of 10°−90°. With an increase in the heat transfer rate, the impact of the tilt angle on the condensation thermal resistance can be detected at higher tilt angles. Indeed, at heat transfer rates from 400 W to 800 W, an increase in the condensation thermal resistance is detected once the angle is reduced below 20°. Furthermore, this increase becomes larger, and the condensation thermal resistance of the multi-channel flat heat pipe evolves by 0.0008 K/W at 800 W, whereas it was only increasing by 0.0003 K/W at 200 W. At large heat transfer rates in the range 900 W−1500 W, the condensation thermal resistance of the multi-channel flat heat pipe increases when the tilt angle decreases below 45°. This variation is at a maximum at 1500 W where, between a tilt angle of 90° and 2°, the condensation thermal resistance of the heat pipe increases from 0.0018 K/W to 0.0038 K/W.

The heat pipe temperatures were studied in order to explain the observed increase in the condensation thermal resistance at low tilt angles. It was observed that this increase is mainly due to a lower temperature at the condenser, whereas the adiabatic temperature remained unchanged. A potential hypothesis for this phenomenon can be the difficulty of the vapour to rise to the condenser, a more important rising vapour/falling liquid film interaction would reduce the vapour passage in the channels, or the difficult formation of a falling film on the top surface of the heat pipe, which would tend to fall on the bottom surface only.

In order to study the impact of the tilt angle on the total thermal resistance of the multi-channel flat heat pipe, the analysis has been divided into three graphs for low, medium, and high heat transfer rates for the sake of clarity, as presented in Fig. 13.

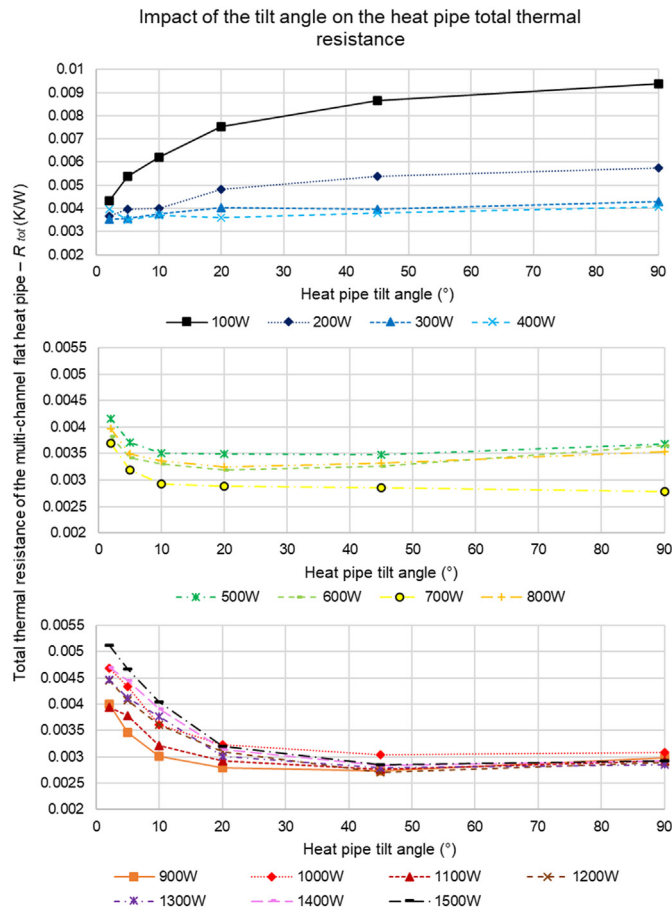At low heat transfer rates, changing the tilt angle of the multi-

Fig. 13. Impact of the tilt angle on the multi-channel flat heat pipe total thermal resistance for low, medium, and high heat transfer rates.
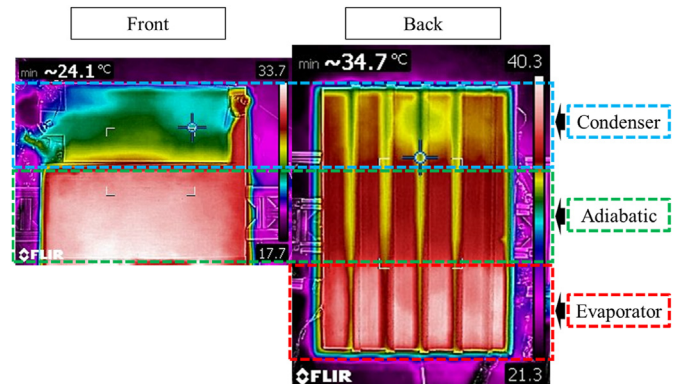

Fig. 14. Infrared imaging of the multi-channel flat heat pipe surface with cooling manifold at the top.

channel flat heat pipe has a significant impact on the boiling thermal resistance but a very small impact on the condensation thermal resistance. Hence, at heat transfer rates of 100 W and 200 W, the total thermal resistance of the heat pipe is at a minimum near the horizontal position and at a maximum in a vertical position. The increase in the total thermal resistance of the heat pipe with the angle at low heat transfer rates is related to the low boiling activity and the important impact of the tilt angle on the natural convection boiling regime. With an increase in the heat transfer rate, this impact reduces as the boiling transits to a fully developed nucleate pool boiling regime. Then, from a heat transfer rate of 400 W, the increase in the thermal resistance of the heat pipe due to the boiling thermal resistance becomes insignificant. However, at low tilt angles, the increase of the condensation thermal resistance impacts the total thermal resistance of the multi-channel heat pipe. At medium heat transfer rates in the range 500 W−800 W, the total thermal resistance of the heat pipe is relatively small and occurs at tilt angles lower than 10° only. However, at higher heat transfer rates, an increase in the total thermal resistance of the multi-channel flat heat pipe is observed at tilt angles lower than 20°. For instance, at a heat transfer rate of 1500 W, the total thermal resistance of the heat pipe increases by 0.002 K/W below 20°, which represents an increase of 66% compared to the vertical position.

6.3. Infrared imaging of the multi-channel flat heat pipe surface

Infrared imaging of the flat heat pipe surface has been conducted using infrared camera FLIR C2 in order to verify the uniform temperature distribution of the multi-channel flat heat pipe. The heat transfer rate was set to a value of 1000 W and the cooling water flow rate to 3 L/min which allows significant temperature differences inside the flat heat pipe system to make the observation easier. The accuracy of the temperature measurements from the infrared imaging has been compared with thermocouple's measurements and it was concluded that the accuracy of the infrared imaging temperature is comparable to the accuracy from thermocouples. Indeed, the infrared imaging accuracy was sufficient to detect colder zones on the condenser that were also detected by thermocouples. The emissivity setting was automatically adjusted by the infrared camera. The heat pipe surfaces were covered with masking tape to prevent reflection from the aluminium. Fig. 14 presents the infrared imaging of the front and back heat pipe surfaces.

The left-hand side of Fig. 14 presents the front surface of the multi-channel flat heat pipe with the adiabatic section and the cooling manifold at the top. As the silicon heaters were placed on the front surface and showed a high temperature, those were kept insulated to allow the observation of the heat pipe surface. From the front heat pipe surface, it is observed that the adiabatic section of the multi-channel flat heat pipe presents a uniform temperature. However, due to the presence of the heaters and cooling manifold on the front surface of the heat pipe, the evaporator and condenser sections can only be observed from the back surface of the heat pipe. On the cooling manifold surface, a temperature gradient corresponding to the warmup of the cooling water is observed with cold water at the top of the manifold and warm water at the bottom. A higher temperature zone in the middle of the cooling manifold is identified and this is discussed later. Regarding the back surface of the multi-channel flat heat pipe, vertical cold lines can be observed, and these correspond to the supports of the heat pipe which are inactive metal plates. At the bottom of the back heat pipe surface, the evaporator section can be visualized. From the infrared imaging, the temperature distribution of the evaporator section is verified, and no hot spot can be identified. A similar conclusion can be made on the adiabatic section which presents a uniform temperature slightly lower than that of the evaporator. At the top of the back surface, the condenser section presents an interesting gradient. Indeed, over the whole cooling manifold surface where the heat is extracted, a cold circle can be visualized at the centre of the condenser and this indicates that more heat is extracted in this zone. After further investigations presented later in the manuscript, it was discovered that this cold spot was created by a better contact between the heat pipe and cooling manifold due to the local adherence of the thermal paste.

From Fig. 14, it was observed that, when the cooling manifold is placed on the top of the multi-channel flat heat pipe, the temperature distribution is uniform. Indeed, due to the direction of the vertical channels, the thermal energy can be easily transported from bottom to top. However, one can wonder if the multi-channel
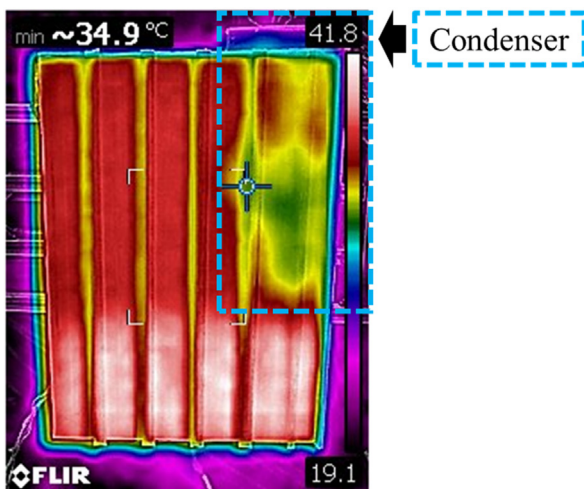

Fig. 15. Infrared imaging of the multi-channel flat heat pipe surface with cooling manifold on the right side.
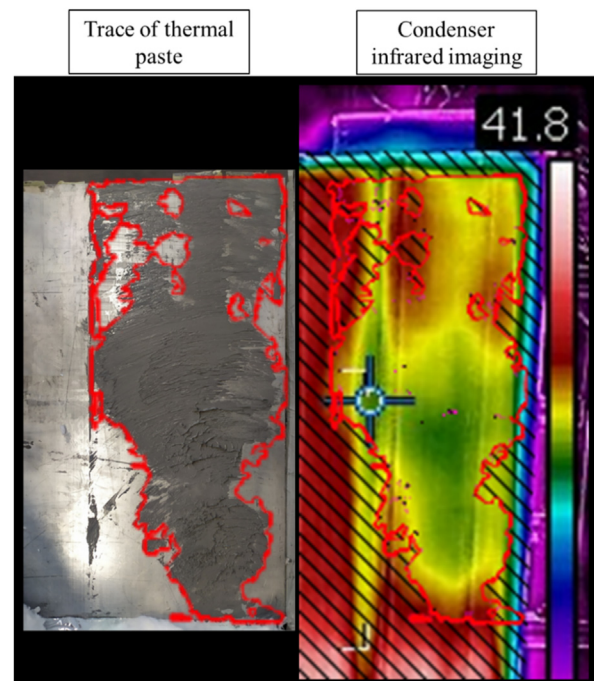

Fig. 16. Comparison of the traces of thermal paste on the heat pipe with the infrared imaging of the condenser.

flat heat pipe is also capable of evenly spreading the energy in a direction perpendicular to the channel's direction. To investigate this aspect, a second experiment was made while the cooling manifold was placed on the side of the heat pipe surface. As such, the capacity of the heat pipe to transfer the heat to a heat sink situated on the right side is investigated, and the back heat pipe surface observed is shown in Fig. 15.

When the cooling manifold is placed on the side of the multi-channel flat heat pipe, the infrared imaging reveals that the evaporator and condenser sections remain completely uniform. Regardless of the proximity with the cooling manifold, the right side of the evaporator presents a similar temperature to the left side. As for the adiabatic section, it can be seen that no accumulation of heat is observed on the top-left corner of the heat pipe. For those two reasons, it is confirmed that the multi-channel internal structure of the heat pipe allows the heat transfer to occur in both vertical and horizontal axes. In addition, such heat transfer rate takes place while maintaining a constant temperature of the sections. On the condenser section, as was observed when the cooling manifold was placed on the top, a cold spot can be identified, and the temperature profile is not uniform. In the case where the cooling manifold was placed on the right, the cold spot is situated in the centre and bottom of the cooling manifold. When the cooling manifold was removed from flat heat pipe surface, despite the fact that the manifold was completely covered by thermal paste, it was observed that the thermal paste had a better adherence with the heat pipe surface at some locations. Interestingly, the traces of thermal paste that remained on the heat pipe surface were compared with the infrared imaging. This is presented in Fig. 16.

In Fig. 16, the red contour of the traces of thermal paste have been superimposed on the infrared imaging of the condenser. The similarity between the traces of thermal paste left on the heat pipe surface and the cold spot of the condenser is easily identified. Hence, it is concluded that the cold spots observed on the condenser section of the flat heat pipe are due to a better adherence of the thermal paste locally. This observation highlights the importance of the interface between the heat pipe and cooling manifold which directly impacts the heat transfer and temperature profile between the heat pipe and the heat sink.

7. Conclusions

In this manuscript, the impact of the heat transfer rate on the thermal performance of a multi-channel flat heat pipe was investigated. A multi-channel thermal resistance model was developed and its capability of predicting the heat pipe thermal resistance at different heat transfer rates was studied. The theoretical model considers the multi-channel geometry of the heat pipe and, by using the correlations by *Rohsenow* and *Hussein* et al. for the pool boiling and condensation heat transfer coefficients, the proposed theoretical model was able to predict the thermal resistance of the heat pipe with an average error of 13.1%. The boiling and condensation thermal resistances were predicted with an error of 17.2% and 14.4%, respectively. Further investigations regarding the impact of the tilt angle on the thermal performance of the multi-channel flat heat pipe have been conducted and revealed that, at low heat transfer rate, the tilt angle of the heat pipe has a high impact on the boiling thermal resistance and a low impact on the condensation thermal resistance. At higher heat transfer rates, the opposite is observed, with a low impact of the tilt angle on the boiling thermal resistance and a high impact on the condensation resistance. Finally, infrared imaging of the multi-channel flat heat pipe surface was conducted and attest that the internal multi-channel geometry of the heat pipe allows an efficient heat transfer in both vertical and horizontal directions, while maintaining a uniform surface temperature at the evaporator and adiabatic sections. At the condenser sections, cold zones were identified due to a local improved adherence of the thermal paste.

Unlike previously conducted research, this manuscript focused on the thermal performances of the multi-channel flat heat pipe itself rather than on its surface cooling application. It is believed that the investigations carried out permitted to improve our fundamental understanding of the two-phase heat transfer occurring inside multi-channel flat heat pipes. This aims at developing further this promising technology and optimizing its design and thermal performances. As a result, in a near future, multi-channel flat heat pipes are expected to extract and recover thermal energy from flat surfaces while reaching unmatched efficiencies. Such innovative thermal absorber can represent a breakthrough for the cooling of flat surfaces such as Photovoltaic/Thermal (PV/T) or battery temperature management applications.

Declaration of competing interest

The authors declare that they have no known competing financial interests or personal relationships that could have appeared to influence the work reported in this paper.

Acknowledgements

References

[1] Jouhara H, Chauhan A, Nannou T, Almahmoud S, Delpech B, Wrobel LC. Heat pipe based systems - advances and applications. Energy Jun. 2017;128: 729–54. https://doi.org/10.1016/J.ENERGY.2017.04.028.

[2] Jouhara H, et al. Applications and thermal management of rechargeable batteries for industrial applications. Energy; Mar. 2019. p. 849–61. https://doi.org/10.1016/j.energy.2018.12.218.

[3] Jouhara H, Serey N, Khordehgah N, Bennett R, Almahmoud S, Lester SP. Investigation, development and experimental analyses of a heat pipe based battery thermal management system. Int. J. Thermofluids Nov. 2019:100004. https://doi.org/10.1016/j.ijft.2019.100004.

[4] Jouhara H, et al. The performance of a novel flat heat pipe based thermal and PV/T (photovoltaic and thermal systems) solar collector that can be used as an energy-active building envelope material. Energy Aug. 2016;108:148–54. https://doi.org/10.1016/J.ENERGY.2015.07.063.

[5] Olabi AG. 100% sustainable energy. Energy Dec. 2014;77:1–5. https://doi.org/10.1016/J.ENERGY.2014.10.083.

[6] Deng Y, Quan Z, Zhao Y, Wang L, Liu Z. Experimental research on the performance of household-type photovoltaic–thermal system based on micro-heat-pipe array in Beijing. Energy Convers Manag Dec. 2015;106:1039–47. https://doi.org/10.1016/J.ENCONMAN.2015.09.067.

[7] Hou L, Quan Z, Zhao Y, Wang L, Wang G. An experimental and simulative study on a novel photovoltaic-thermal collector with micro heat pipe array (MHPA-PV/T). Energy Build Jul. 2016;124:60–9. https://doi.org/10.1016/J.ENBUILD.2016.03.056.

[8] Modjinou M, Ji J, Li J, Yuan W, Zhou F. A numerical and experimental study of micro-channel heat pipe solar photovoltaics thermal system. Appl Energy Nov. 2017;206:708–22. https://doi.org/10.1016/j.apenergy.2017.08.221.

[9] Shittu S, Li G, Zhao X, Zhou J, Ma X, Akhlaghi YG. Experimental study and exergy analysis of photovoltaic-thermoelectric with flat plate micro-channel heat pipe. Energy Convers Manag Mar. 2020;207:112515. https://doi.org/10.1016/j.enconman.2020.112515.

[10] Yu M, et al. Experimental investigation of a novel solar micro-channel loop-heat-pipe photovoltaic/thermal (MC-LHP-PV/T) system for heat and power generation. Appl Energy Dec. 2019;256:113929. https://doi.org/10.1016/j.apenergy.2019.113929.

[11] Jouhara H, et al. The performance of a heat pipe based solar PV/T roof collector and its potential contribution in district heating applications. Energy Oct. 2017;136:117–25. https://doi.org/10.1016/J.ENERGY.2016.04.070.

[12] Kim G-H, Pesaran A. Battery thermal management design modeling. World Electr. Veh. J. 2007;1(1):126–33.

[13] Diao YH, Liang L, Zhao YH, Wang ZY, Bai FW. Numerical investigation of the thermal performance enhancement of latent heat thermal energy storage using longitudinal rectangular fins and flat micro-heat pipe arrays. Appl

Energy Jan. 2019;233(234):894–905. https://doi.org/10.1016/j.apenergy.2018.10.024.

[14] Zhao R, Gu J, Liu J. An experimental study of heat pipe thermal management system with wet cooling method for lithium ion batteries. J Power Sources Jan. 2015;273:1089–97. https://doi.org/10.1016/j.jpowsour.2014.10.007.

[15] Almahmoud S, Jouhara H. Experimental and theoretical investigation on a radiative flat heat pipe heat exchanger. Energy May 2019;174:972–84. https://doi.org/10.1016/J.ENERGY.2019.03.027.

[16] Almahmoud S. Experimental and theoretical investigation on a radiative flat heat pipe heat exchanger for waste recovery in the steel industry. Brunel University London; 2019.

[17] Delpech B, Axcell B, Jouhara H. Experimental investigation of a radiative heat pipe for waste heat recovery in a ceramics kiln. Energy Mar. 2019;170: 636–51. https://doi.org/10.1016/J.ENERGY.2018.12.133.

[18] Guichet V, Khordehgah N, Jouhara H. Experimental investigation and analytical prediction of a multi-channel flat heat pipe thermal performance. Int. J. Thermofluids Jul. 2020:100038. https://doi.org/10.1016/j.ijft.2020.100038.

[19] Jouhara H, Lester S. Heat transfer apparatus. 2015, WO2015193683.

[20] Guichet V, Almahmoud S, Jouhara H. Nucleate pool boiling heat transfer in wickless heat pipes (two-phase closed thermosyphons): a critical review of correlations. Therm Sci Eng Prog 2019;13. https://doi.org/10.1016/j.tsep.2019.100384.

[21] Guichet V, Jouhara H. Condensation, evaporation and boiling of falling films in wickless heat pipes (two-phase closed thermosyphons): a critical review of correlations. Int. J. Thermofluids 2020;1–2. https://doi.org/10.1016/j.ijft.2019.100001.

[22] Rohsenow WM. A method of correlating heat-transfer data for surface boiling of liquids. 1952. Accessed: Jan. 26, 2019. [Online]. Available: http://iibraries.mit.edu/docs.

[23] Nusselt W. The condensation of steam on cooled surfaces. Z. Ver. Dtsch. Ing 1916;60:541–6.

[24] Cengel YA. Heat transfer: a practical approach. New York McGraw-Hill; 2003. p. 785–841. https://doi.org/10.1017/CBO9781107415324.004.

[25] Kruzhilin GN. Free-convection transfer of heat from a horizontal plate and boiling liquid. Dokl. AN SSSR (Reports USSR Acad. Sci. 1947;58(8):1657–60.

[26] McNelly MJ. A correlation of rates of heat transfer to nucleate boiling of liquids. J. Imp. Coll. Chem. Eng. Soc 1953;7:18–34.

[27] Forster HK, Zuber N. Dynamics of vapor bubbles and boiling heat transfer. AIChE J 1955;1(4):531–5.

[28] Tien CL. A hydrodynamic model for nucleate pool boiling. Int J Heat Mass Tran Jun. 1962;5(6):533–40. https://doi.org/10.1016/0017-9310(62)90164-3.

[29] Lienhard JH. A semi-rational nucleate boiling heat flux correlation. Int J Heat Mass Tran Mar. 1963;6(3):215–9. https://doi.org/10.1016/0017-9310(63)90108-X.

[30] Mostinkski IL. Application of the rule of corresponding states for calculation of heat transfer and critical heat flux. Teploenergetika 1963;4(1963):66–71.

[31] Mikic BB, Rohsenow WM. A new correlation of pool-boiling data including the effect of heating surface characteristics. J Heat Tran May 1969;91(2):245–50. https://doi.org/10.1115/1.3580136 [Online]. Available:.

[32] Danilova GN. Correlation of boiling heat transfer data for Freons. Heat Tran Res 1970;2(2):73–8.

[33] Labuntsov DA. Heat transfer problems with nucleate boiling of liquids. Therm Eng(USSR)(Engl Transl) 1973;19(9):21–8.

[34] Imura H, Kusuda H, Ogata J-I, Miyazaki T, Sakamoto N. Heat transfer in two-phase closed-type thermosyphons. JSME Trans 1979;45:712–22.

[35] Stephan K, Preusser P. Wrmebergang und maximale wrmestromdichte beim behiterienden binrer und ternrer flussigkeitsgemische. Chem Ing Tech 1979;51.1:1–37.

[36] Stephan K, Abdelsalam M. Heat-transfer correlations for natural convection boiling. Int J Heat Mass Tran Jan. 1980;23(1):73–87. https://doi.org/10.1016/0017-9310(80)90140-4.

[37] Shiraishi M, Kikuchi K, Yamanishi T. Investigation of heat transfer characteristics of a two-phase closed thermosyphon. J Heat Recovery Syst Jan. 1981;1(4):287–97. https://doi.org/10.1016/0198-7593(81)90039-4.

[38] Bier K, Schmadl J, Gorenflo D. Influence of heat flux and saturation pressure on pool boiling heat transfer of binary mixtures. VT VERFAHRENSTECHNIK 1982;16(9):708–10.

[39] Nishikawa K, Fujita Y, Ohta H, Hidaka S. Effect of the surface roughness on the nucleate boiling heat transfer over the wide range of pressure. In: Heat transfer, proceedings of the international heat transfer conference; 1982. p. 61–6.

[40] Cooper MG. Saturation nucleate pool boiling - a simple correlation. Inst. Chem. Eng. Symp. Ser. Jan. 1984;2(86):785–93. https://doi.org/10.1016/B978-0-85295-175-0.50013-8.

[41] Ueda T, Miyashita T, Chu P-H. Heat transport characteristics of a closed two-phase thermosyphon, vol. 54; 1988.

[42] Kutateladze SS. Heat transfer and hydrodynamic resistance: handbook (in Russian), chapter 12.7. Moscow: Energoatomizdat Publishing House; 1990.

[43] Groß U. Pool boiling heat transfer inside a two-phase thermosyphon (correlation of experimental data). In: Proc. 9th int. Heat transfer conf., 1990, vol. 2; 1990. p. 57–62.

[44] Gorenflo D, Sokol P, Caplanis S. Pool boiling heat transfer from single plain tubes to various hydrocarbons. Int J Refrig Sep. 1990;13(5):286–92. https://doi.org/10.1016/0140-7007(90)90059-6.

[45] Kaminaga F, Okamoto Y, Suzuki T, Ma T. Study on boiling heat transfer correlation in a closed two-phase thermosyphon. 1992.

[46] Leiner W. Heat transfer by nucleate pool boiling—general correlation based on thermodynamic similarity. Int J Heat Mass Tran Mar. 1994;37(5):763–9. https://doi.org/10.1016/0017-9310(94)90114-7.

[47] Leiner W, Gorenflo D. Methods of predicting the boiling curve and a new equation based on thermodynamic similarity. Pool Extern. Flow Boil. 1992: 99–103.

[48] Chowdhury FM, Kaminaga F, Goto K, Matsumura K. Boiling heat transfer in a small diameter tube below atmospheric pressure on a natural circulation condition. J. Japan Assoc. Heat Pipe 1997;16(1997):14–6.

[49] El-Genk MS, Saber HH. Heat transfer correlations for small, uniformly heated liquid pools. Int J Heat Mass Tran 1997;41(2):261–74. https://doi.org/10.1016/S0017-9310(97)00143-9.

[50] Kiatsiriroat T, Nuntaphan A, Tiansuwan J. Thermal performance enhancement of thermosyphon heat pipe with binary working fluids. Exp. Heat Transf. 2000;13(2):137–52. https://doi.org/10.1080/089161500269517.

[51] Ribatski G, Jabardo JMS. Experimental study of nucleate boiling of halocarbon refrigerants on cylindrical surfaces. Int J Heat Mass Tran Nov. 2003;46(23): 4439–51. https://doi.org/10.1016/S0017-9310(03)00252-7.

[52] McAdams WH. Heat transmission. second ed. New York: McGRAW; 1942.

[53] Rohsenow WM. Heat transfer and temperature distribution in laminar film condensation. Trans. Asme 1956;78:1645–8.

[54] Kutateladze SS. Heat transfer theory fundamentals. Atomizdat, moscow./E. Arnold publishers, london. New York: Academic Press Inc; 1963.

[55] Butterworth C. Condensers: basic heat transfer and fluid flow. Kakaç, S.; Bergles, AE; Mayinger, F. Heat Exch. Therm. Fundam. Des. Washingt. Hemisph. 1981:289–313.

[56] Wang JCY, Ma Y. Condensation heat transfer inside vertical and inclined thermosyphons. J Heat Tran Aug. 1991;113(3):777–80.

[57] Gross U. Reflux condensation heat transfer inside a closed thermosyphon. Int J Heat Mass Tran Feb. 1992;35(2):279–94. https://doi.org/10.1016/0017-9310(92)90267-V.

[58] Schnabel G, Palen JW. Wärmeubergang an senkrechten berieselten Flächen. Berlin: Springer-Verlag Sect. Md.; 1998.

[59] Hussein HMS, Mohamad MA, El-Asfouri AS. Theoretical analysis of laminar-film condensation heat transfer inside inclined wickless heat pipes flat-plate solar collector. Renew Energy Jul. 2001;23(3–4):525–35. https://doi.org/10.1016/S0960-1481(00)00149-X.

[60] Fiedler S, Auracher H. Experimental and theoretical investigation of reflux condensation in an inclined small diameter tube. Int J Heat Mass Tran Sep. 2004;47(19–20):4031–43. https://doi.org/10.1016/J.IJHEATMASSTRANSFER.2004.06.005.

[61] Uehara H, Kusuda H, Nakaora T, Yamada M. Filmwise condensation for turblent flow in a vertical tube. Heat Transf. Japanese Res. 1983;12(2):85–96.

[62] Chun MH, Kim KT. A natural convection heat transfer correlation for laminar and turbulent film condensation on a vertical surface. In: 3rd ASME/JSME thermal engineering joint conference; 1991. p. 459–64.

[63] Nozhat WM. The effect of free surface curvature on the heat transfer coefficient of thin liquid films. In: Fourth American society of mechanical engineers/Japanese society of mechanical engineers thermal engineering joint conference, maui, hawaii, vol. 2; 1995. p. 171–8.

[64] Hashimoto H, Kaminaga F. Heat transfer characteristics in a condenser of closed two-phase thermosyphon: effect of entrainment on heat transfer deterioration. Heat Tran Res May 2002;31(3):212–25. https://doi.org/10.1002/htj.10030.

[65] Jouhara H, Robinson AJ. Experimental investigation of small diameter two-phase closed thermosyphons charged with water, FC-84, FC-77 and FC-3283. Appl Therm Eng Feb. 2010;30(2–3):201–11. https://doi.org/10.1016/J.APPLTHERMALENG.2009.08.007.

[66] Labuntsov DA. Heat transfer in film condensation of pure steam on vertical surfaces and horizontal tubes. Teploenergetika 1957;4(7):72–9.